

UNIVERSITY OF PISA

COURSE OF STUDY IN SPACE ENGINEERING
Department of Mechanical and Industrial Engineering



A Theoretical and Experimental Investigation on a Solenoid Valve for Space Applications

Final Thesis of the Space Engineering Course

Relator:

Prof.

Paganucci Fabrizio

Written by:

Bambagioni Fabio

Academic Year
2015/2016

Abstract

As the space journeys seems to become more diffuse and achievable, the manufacturers of the on-board system strive to reduce the cost and increase the reliability of their products, so the dimensions optimization of each parts of these system will gain increasing importance.

In this thesis, an innovative type of solenoid valve has been investigated and optimized. Due to the highly non-linear physical relationships inherent to electromagnetic devices, design and control of these valves has proven to be exceptionally challenging. To better predict valve performances, before that it was tested with experiments, a parametric code regarding the main aspects of the valve has been developed using the software *MatlabTM* and validated on an existing physical prototype.

This study has demonstrated that this innovative valve could be implemented in a Xenon Feeding System with positive consequences in terms of power consumption or space occupied, provided that a properly configuration has been selected and developed. The simulation and the experimental results have been matched well and this work could be taken as a starting point for future design purposes.

Acknowledgements

I would like to express profound thankfulness to my supervisor Paganucci Fabrizio, Professor at the university of Pisa, for his invaluable support and useful suggestions throughout this research work. His willingness to share his time so generously has been very much appreciated.

I wish to extend my sincere gratitude to Scortecci Fabrizio for providing me the opportunity to develop this work in "Aerospazio tecnologie s.r.l.", and I would specially thank Sestini Leonardo for his technical assistance with the valve's prototypes and the experimental set up.

The completion of this journey could not have been accomplished without the support of my classmates, Luca, Jacopo, Daniel, Federico and Lorenzo.

Last but not least, I would like to express my heartfelt thank to my caring family for its support support and encouragement throughout my studies.

Contents

1	Introduction	1
1.1	State of the Art	1
1.2	Xenon Feeding Systems	4
1.3	Cold Gas Thruster	7
1.3.1	Cold Gas Propellants	8
1.4	Thesis Approach	10
2	Mathematical Model	13
2.1	Data Collected	13
2.2	Physical Model	15
2.3	Model Assumptions	16
2.4	Electrical Model	17
2.4.1	Electrical Circuit	17
2.4.2	Electrical Equations	18
2.4.3	Inductance Analysis	19
2.5	Magnetic Model	21
2.5.1	Magnetic Circuit	21
2.5.2	Magnetic Equations	23
2.5.3	Second Order Analysis	24
2.6	Mechanical Model	28
2.7	Hydrodynamics Model	30
2.8	Heating Equations	33
2.9	Model Summary	35

3 Valve Optimization	37
3.1 Design Approach	37
3.2 Spring Modifications	38
3.3 Coil Case Modifications	40
3.4 Main Case Modifications	42
3.5 Main Body Front Case Modifications	44
3.5.1 Micro O-ring Implementation	45
3.6 Assembly Comparison	48
3.7 Coil Modifications	50
3.7.1 Pick and Hold Strategy	51
4 Simulations and Models	53
4.1 Procedure of Development	53
4.2 First Order Codes	55
4.2.1 Electric Code	55
4.2.2 Spring Code	57
4.2.3 Magnetic Code	59
4.2.4 Heating Code	61
4.3 Main Codes	63
4.3.1 Power Fixed Code	63
4.3.2 Ampere-Spire Fixed Code	65
4.4 Empirical Coefficient	67
5 Tests and Apparatus	69
5.1 Vacuum Apparatus	69
5.1.1 Vacuum Gauges	69
5.1.2 Leak Detector	71
5.1.3 Vacuum Chamber	72
5.2 Experiments Set Up & Results	74
5.2.1 Leak Rate Evaluation	74
5.2.2 Minimum Force Identification	78
5.2.3 Temperature Rising Experiment	82

Conclusions	92
A High Vacuum Gauges	93
A.1 Hot Cathode Gauge (HCG)	94
A.2 Cold Cathode Gauge (CCG)	96
A.3 Residual Gas Analyzer (RGA)	97
B Matlab codes	99
B.1 Electric Circuit Code	99
B.1.1 Electric Function	99
B.1.2 Electric Editor	100
B.2 Spring Force	102
B.3 Magnetic Force	104
B.4 Heating Effect	106
B.5 Final Code	109
Bibliography	115

List of Figures

1.1	Solenoid Valve Scheme	2
1.2	Direct Acting Solenoid Valve	3
1.3	Internally piloted solenoid valve	3
1.4	Scheme of Xenon Feed System	5
1.5	Scheme of CGT system	7
2.1	Valve Physical Scheme	15
2.2	Electric Circuit Scheme	17
2.3	Current-Time graph	18
2.4	Valve Section	21
2.5	Vacoflux Magnetization Curve	22
2.6	Movable Magnet Section	25
2.7	Detailed Magnetic Circuit	26
2.8	Forces Equilibrium Scheme	28
2.9	Geometry Analysis of the Seal mechanism	31
3.1	First Version Spring	38
3.2	Modified Spring	39
3.3	First Version Coil Case	40
3.4	Modified Coil Case	41
3.5	First Version Main Case	42
3.6	Modified Main Case	43
3.7	First Version Main Body Front Case	44
3.8	Modified Main Body Front Case	45

3.9	MicrOring Table	47
3.10	First Version Dimensions	48
3.11	Modified Version Dimensions	49
3.12	Pick and Hold Graph	51
4.1	RL Circuit Simulation Example	55
4.2	RL Circuit Simulation Graph	56
4.3	Spring Simulation Example	57
4.4	Spring Simulation Graph	58
4.5	Magnetic Force Simulation Example	59
4.6	Magnetic Force Simulation Graph	60
4.7	Heating Simulation Example	61
4.8	Heating Simulation Graph	62
4.9	Power Fixed, Electric Simulation	63
4.10	Power Fixed, Magnetic Simulation	64
4.11	Ampere-Spore Fixed, Electric Simulation	65
4.12	Ampere-Spore Fixed, Magnetic Simulation	66
5.1	Operational Ranges of Vacuum Gauges	71
5.2	Medium Vacuum Chamber	73
5.3	First Experiment Scheme	75
5.4	Leak Rate Experiment	76
5.5	First Coil Configuration 0,56 mm	78
5.6	Second Coil Configuration 0,8 mm	79
5.7	Second Experiment Set Up	80
5.8	Temperature Experiment Air Set Up	83
5.9	Temperature Fitting in Air	85
5.10	Temperature Experiment Vacuum Set Up	86
5.11	Temperature Fitting in Vacuum	87
5.12	Scheme of Thermocouple Positioning	89
5.13	Average Temperature in Air and in Vacuum	90
A.1	Hot Cathode Gauge Scheme	94

A.2 Gas Correction Factor	96
A.3 Cold Cathode Gauge Scheme	97

List of Tables

1.1	Propulsion Systems Tasks	8
1.2	Gas Propellants Performances	8
2.1	Standard Parameters for Solenoid Valve	14
5.1	Leak Rate Results	76
5.2	Minimum Amperage for Opening	80
5.3	Temperature Rising Results in Air for 1,15 A	84
5.4	Temperature Rising Results in Air for 2,3 A	84
5.5	Temperature Rising Results in Air for 2,55 A	84
5.6	Temperature Rising Results in Vacuum	87
5.7	Temperature Rising Comparison	88

Chapter 1

Introduction

In this chapter the actual "state of art" of solenoid valve's technology and their working mechanism are briefly described. Then the work environments and the tasks for which this valve has been thought are presented. In the end the approach used to study and modify the valve is explained.

1.1 State of the Art

The solenoid valves are widely used in the aerospace industry for several reason, first of all their versatility which allows them to cover different roles depending on the designer needs. Solenoid valves work electromechanically, in fact they use a magnetic force, generated by a coil, to move a ferromagnetic core. The core consequently opens or closes the valve, permitting or interrupting the transition of the fluid. Usually the ferromagnetic core is orthogonal to fluid's flux and it passes in the internal part of a hollow cylinder. The position of the core is regulated by the magnetic field generated by the coil. A spring attracts the ferromagnetic core when the coil is at rest and the fluid is not allowed to flow. When the coil is activated, and a current passes through it, a magnetic force is employed on the ferromagnetic core. If this force is big enough, it can win the elastic force of the spring and the fluid is permitted to flow. A scheme of this type of valves is illustrated in figure 1.1.

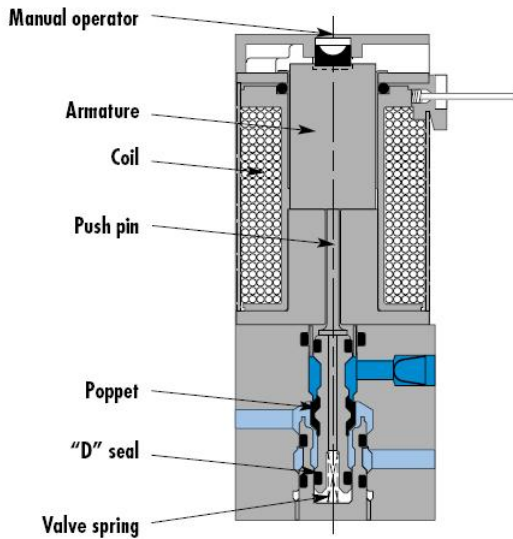


Figure 1.1: Solenoid Valve Scheme

We need to spend few words about the role of the coil. Firstly it must generate a minimum force that allow the movement of the ferromagnetic core. Then in order to guarantee an appropriate fluid's flow, this force must allow the ferromagnetic core to reach the desired position. In the worst case, the coil doesn't generate a force intense enough to permit the movement of the ferromagnetic core and the fluid can't flow. When the valve is at rest, the spring has to guarantee the seal of the valve in order to inhibit the flowing of the fluid. Obviously it must be designed together the coil so that the valve works properly.

Solenoid valves are characterized by how they operate. If the force generated by the solenoid is sufficient to open the valve, this can be named direct acting solenoid valve. The force generated by the solenoid acts directly on the fluid as it can be seen in figure 1.2.

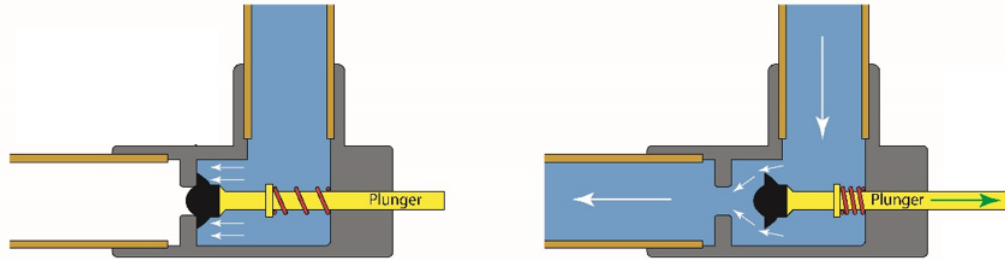


Figure 1.2: Direct Acting Solenoid Valve

If the pressure is higher or the orifice larger we require an higher force. In order to reach this force, we have to design an internally piloted solenoid valve. In these valves the solenoid is used to control a line pressure that generate the high valve forces.

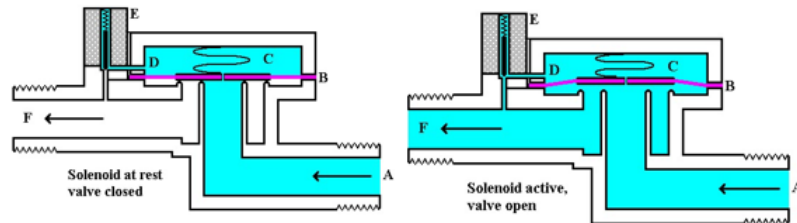


Figure 1.3: Internally piloted solenoid valve

The valves described up to now belong to the class of the mono-stable valves. These have a position of equilibrium at rest only when the coil is turned off, whereas when we activate the coil the valves reach the equilibrium position, but they are able to maintain it just until the coil works.

Another class of valves is named bi-stable valves. These have two positions of equilibrium and both can be maintained even if the coil is turned off. As disadvantages these valves need two coils and a bigger availability of volume.

1.2 Xenon Feeding Systems

In order to understand the first task that our valve must fulfill, it has to be clear how a Xenon Feed System (XFS) works.

There are two types of thruster assemblies which can use this system: electric propulsion thrusters with typical Xenon flow rate requirements of 0.1-10 mg/s and cold gas thrusters which flow rate is one or two order of magnitude higher. The total system needs always of a Power Processing Unit (PPU), that takes the power directly from the power generator and delivers it from a primary regulated bus the electrical power to the various parts of the valve, and of a Digital Control and Interface Unit (DCIU), with the purpose of collecting, driving and monitoring the data not only from the thruster but also from all the components that allow it to work. These units are two physically independent units that work as one, so sometimes are thought as unitary component.

The main function of the Xenon Feed System are:

- To supply a constant feed pressure to the thruster assemblies.
- To decrease the Xenon pressure from inlet tank pressure down to a regulated minimum pressure of 1-5 bar at the outlet (the set point can be changed by controllers).
- To guarantee a total Xenon mass throughput without exceeding cycles qualification limit of the solenoid valves.
- To ensure that the Xenon remains in a gaseous state throughout the passage from the high pressure part to the low pressure part. In fact, the Xenon temperature has to be maintained between 20 °C and 50 °C.

A simple Xenon Feed System for a resistojet is reported in figure 1.4, anyway the basic principles are the same for all electric thruster able to use Xenon as fuel supply.

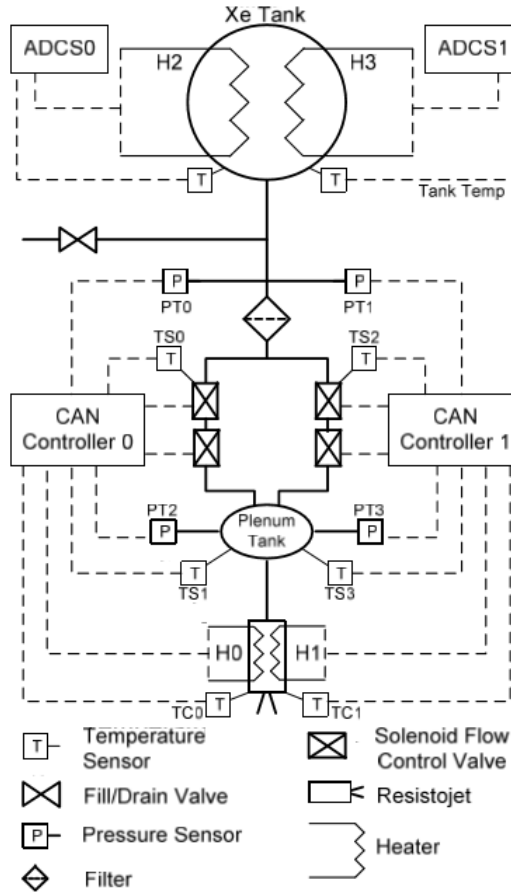


Figure 1.4: Scheme of Xenon Feed System

A well designed feeding system can be supposed divided in two parts, one of high pressure and the other of low pressure. Usually the high pressure part include:

1. Main Xenon tank, it has the function to store the propellant and its nominal pressure is around 150 bar.
2. Mechanical filter which dimensions are in the range of the micron.
3. Fill and drain valve which function is to provide an interface port which will allow accessing to the Xenon Feed System and simultaneously providing a sealing capability between the system and outside environment

at low and high pressure. This valve also shall act as test ports and shall allow the system to be serviced with the leak detection agents necessary for system test.

4. High pressure transducers able to transmit to the Digital Control and Interface Unit information about temperature and pressure.
5. A group of pressure reducers used for plenum tank pressure control. Usually it is done by solenoid valves regulating their opening time depending on the flow rate desired.
6. Latch valve able to connect or isolate the various parts of the circuit and guarantee the switching of the flow through a redundancy circuit in case of failure.

The low pressure part consist of:

1. Secondary tank, usually named "accumulator" or "plenum", is used to improve the control and the accuracy of the mass flow rate.
2. Low pressure transducers.
3. Fill and drain valve.
4. System for the accurate regulation of the mass flow rate, usually are used calibrated orifices or control valves.
5. Low pressure latch valve.

Furthermore the system must be warms up in order to avoid phase change of the Xenon, malfunctions and formation of residual structural stresses given by the temperature variation. This is usually done by heaters attached to the critical parts of the system.

In this system our valve can cover two different role: it can be putted at the exit of the Xenon tank in order to allow or stop the passage of the fluid otherwise it can be used as controller so as to managing the flow rate of the system. In this study has been studied a valve capable to cover the first role listed.

1.3 Cold Gas Thruster

This valve has been thought to be used not only as a component of the XFS, but also, making the minimum modifications, as a Cold Gas Thruster (CGT).

The CGT are commonly used in small satellites for a wide range of earth orbit and even interplanetary missions because of its low cost, encumber and mass. They are the most diffused low thrust space propulsion for LEO maneuvers and their high reliability is confirmed by the fact that they are used since 1960's. These thrusters provide a sufficient amount of force to provide stabilization in pitch, yaw and roll movement of satellite.

The CGT usually are integrated in a system composed by a propellant tank, solenoid valves, thrusters, tubing and fittings. A scheme of this system is reported in the figure below.

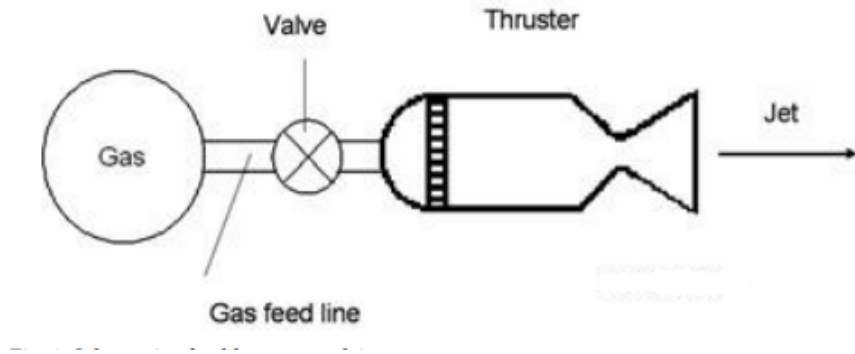


Figure 1.5: Scheme of CGT system

A table with the principal options for a classical space mission is reported in order to clarify which tasks can achieve our CGT.

Propulsion Tecnology	Orbit Insertion	Orbit Manuver	Attitude Control	Specific Impulse
Cold Gas	No	Yes	Yes	30-70
Solid	Yes	No	No	280-300
Liquid	No	Yes	Yes	220-340
Electric	No	Yes	No	300-3000

Table 1.1: Propulsion Systems Tasks

1.3.1 Cold Gas Propellants

As said before one of the main passage for the study of a CTG is the choice of the propellant gas. For this reason a table with the common propellants is reported below.

Propellant Gas	Molecular Weight [kg/kmole]	Density [g/cm ³]	Specific Thrust [s]
Hydrogen	2	0.02	296
Helium	4	0.04	179
Nitrogen	28	0.28	80
Ammonia	17	Liquid	105
Carbon Dioxide	44	Liquid	67

Table 1.2: Gas Propellants Performances

Nitrogen is most commonly used as a cold gas propellant, and it is preferred for its storage density, performance, and lack of contamination concerns. As shown in table below, hydrogen and helium have greater specific impulse as compared to other propellants, but have a low molecular weight. This quality causes an increased tank volume and weight, and ultimately causing an increase in system weight. Carbon dioxide can be a good choice, but due to its toxic nature, it is not considered for cold gas systems. Another

good alternative propellant could be ammonia, which stores in its liquid form to reduce tank volume. Its specific impulse is higher than nitrogen or other propellants and reduces concerns of leakage, although it also necessitates a lower mass flow rate. Despite the benefits, ammonia is not suitable for this system as one alternative to decrease the system size and weight includes pressurizing the satellite and allowing the entire structure to act as a propellant tank, as previously mentioned. In this system, the ammonia could cause damage to electrical components.

1.4 Thesis Approach

In this section the approach used to study the valve is explained. It is presented in the chronological order in which each step has been done and some of the choices done during this the course of this study has been reported.

This work is based on the drawings of a specific solenoid valve received from the company AEROSPAZIO Tecnologie s.r.l. Starting from these drawings the CAD model of the various parts has been done using the environments "Part Design" and "Generative Shape Design" of the software *CATIATM*. Because of the tiny dimensions of some parts graphic problem has been found, in order to avoid them all the parts have been firstly designed in a 10:1 scale and then have been reported in a 1:1 scale. Thereafter, using the environment "Assembly Design" of the same software the CAD model has been assembled. During this phase it has not been possible identify the position of some parts in the final assembly drawing, so the missed parts has been positioned looking at the functional mechanism of the valve and at the coincidences in measurement of various parts.

When the CAD model was completed, a mathematical model has been created. It was necessary a model able to describe the static and the dynamic behavior of the solenoid valve, so it has been searched into the actual literature. From this study it has been decided to separate our system in different parts, analyze each part in detail and finally reunite all these parts in one model. In order to do this various assumption has been made (a list of them can be found in chapter 2).

Then some parts of the valve have been optimized bearing in mind their functional role in the system and avoiding modifications which can corrupt the valve mechanism. Practically the core of the valve has been modified the less as possible, while the external parts, which had the greatest margins of improvements and the risks to compromise its work were lower, has been

completely changed. In the chapter 3 a list of the modified parts and the external views of the two version of the valve can be found.

Thereafter a simulated model has been created in order to have a first idea of the relationship between the different parameters. Firstly some first order codes has been developed describing the principal aspect of the valve's mechanism. Then they has been implemented in just one main code capable to evidence the principal parameters differences for different input. Finally two version of this main code has been derived in order to better interface our codes to the experiments. This part has been developed using the software *MatlabTM*.

The final part regard the experiments that have been developed among the location of the company Aerospazio Tecnologie s.r.l. Firstly various vacuum instruments has been described, then the set up and the results of the experiments have been presented and analyzed. At least some conclusions has been derived and some idea for a future work has been expressed.

Chapter 2

Mathematical Model

In this chapter are presented the equations which describe the dynamics of our system. Initially a physical model describing the physic of the valve has been created and from this, using some assumptions and computation, it has been wrote a system of equations representing the behavior of the valve.

2.1 Data Collected

This phase of the project has started from a collection of data. Initially, data the feeding system and the actual standard for the solenoid valves in commerce has been given to me by Aerospazio Tecnologie s.r.l. After, data were searched on internet, directly into web pages of that companies which have contributed to the creation of these types of valves. It has to be underlined that many data were similar each other.

Once that the order of magnitude of these valves standard parameters has been clarified, a research in the literature of different field of knowledge has been done. The principal areas of study that have been examined in depth were: the physics of electromagnetism and in particular the magnetic circuit, the hydrodynamic of a fluid and the heat exchange in vacuum environment. In any case all the texts used are reported in the bibliography, at the end of the thesis. All these information have been used to build up the following

models.

The values of the standard parameters used to describe the solenoid valve have been reported in the table below, in order to clarify the the order of magnitude of the phenomena involved. We have to precise that the data reported below belong to valves of only one company.

Valve Model	MV100	MV100GD	MV130	MV130H
Proof Pressure[bar]	310	300	310	621
Burst Pressure[bar]	517	800	517	1034
Voltage DC[V]	18 to 30	18 to 32	18 to 30	18 to 30
Current[A]	1	1	1.33	1.33
Resistance[Ohm]	24.5	24	18	18
C_v	0.18	0.25	0.625	0.55
Body Material	Al Alloy	Monel 400	Al Alloy	Al Alloy
Seat Material	Vespel SP-1	Vespel SP-1	Nylon	Vespel SP-1
Seal Material	Buna N	Butyl	Buna N	Isoprene Rubber
Weight[kg]	0.363	0.61	0.61	0.77
Response Time[ms]	< 50	< 50	< 70	< 90

Table 2.1: Standard Parameters for Solenoid Valve

2.2 Physical Model

In order to simplify and schematize the problem a physical model of the system has been created. It can be imagine divided in different parts: an electric circuit belonging to the RL types, a magnetic circuit, a spring and a plunger which directly act on the orifice. In the magnetic circuit there are two magnets separated by an air gap; one of the magnets is fixed and it is wrapped by the solenoid of the electric circuit, whereas the other magnet is mobile and it is attached to the plunger, which is also movable along its stroke. Its motion controls the opening and the closing of the orifice and consequently the passage of the fluid through the valve.

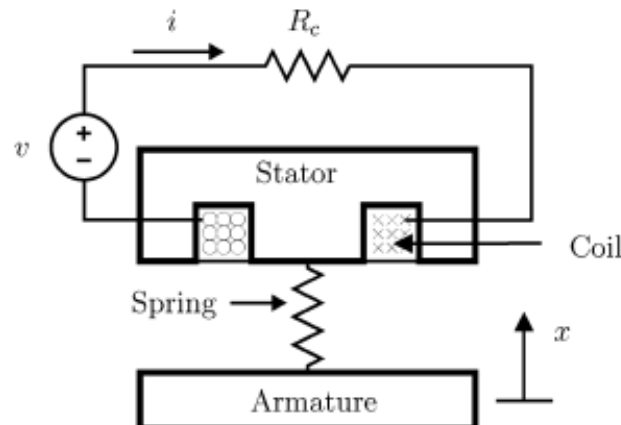


Figure 2.1: Valve Physical Scheme

2.3 Model Assumptions

The description of the system has been simplified using some approximations of different significance. A list of them is now presented in no particular order:

- The solid parts of the system are considered rigid;
- The viscous phenomena are neglected;
- The inductance is approximated as constant;
- The magnetic permeability is assumed linear;
- The effect of eddy current is overlooked;
- The dissipation of the energy occurs only in the spring and in the resistance of the electric circuit as Joule Effect;
- The behavior of the spring considered linear
- The pressure upstream is took constant;
- The work fluid is Xenon and it is considered ideal;
- Other minor assumptions, as for example the simplification of some equations, are shown in the respective sections.

2.4 Electrical Model

In this section the electrical model is presented. Firstly the electric circuit is described and analyzed, then the equations used are listed and explained. The section has been closed with an observation regarding the inductance of the circuit.

2.4.1 Electrical Circuit

In order to analyze the appropriate electric circuit, it has been created a classical RL circuit, where the electric resistance has been put in series with the inductance. As power source a DC voltage generator has been utilized. The following representation has been done using the environment "SimuLink" of the software *MatlabTM*.

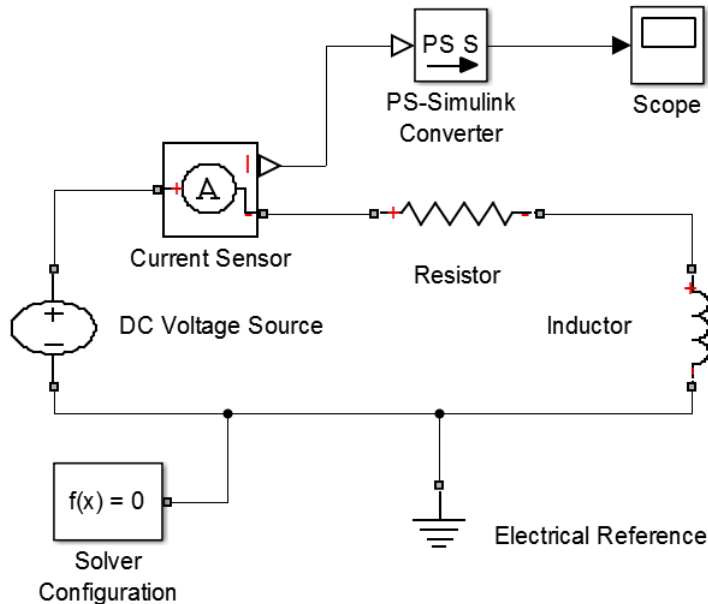


Figure 2.2: Electric Circuit Scheme

The aim of this analysis is the identification of the time necessary to

charge the solenoid. In order to do this, the time constant of the solenoid valve has been computed, it also could be done analytically, solving the classical first order linear differential equation related to the RL circuits. The simulation has been based on the data collected from the various companies. The principal parameters of the system respect the standard ones used in typical solenoid valve. For this example the voltage is been set to 24 V, the current to 1.1 A and the inductance has been computed as 1.5 H bearing in consideration the nature of the ferromagnetic material and the dimension of the coil. The simulation results are reported in figure 2.3.

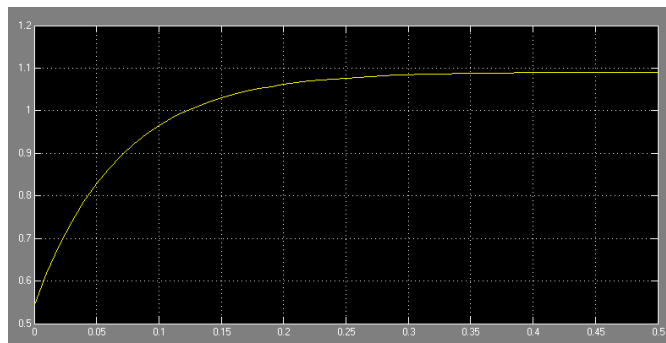


Figure 2.3: Current-Time graph

In order to decrease the value on the time constant a "Pick and Hold" strategy could be used. It practically consist in the giving to the electric circuit an high voltage for a short period of time with the aim to reach earlier the saturation current. Once that the level of current desired has been reached the initial high voltage is substituted which the operating voltage. The heat developed can also cross the melting limit of the material if it is maintained for the right period of time. This method will be examine in the next chapter.

2.4.2 Electrical Equations

From the electric circuit scheme of figure 2.2, using the Faraday's law and Kirchhoff's 2nd law, the equation of the circuit can be written as:

$$V = iR + L \frac{di}{dt} + i \frac{dL}{dt} \quad (2.1)$$

Where V is the difference of voltage applied by the DC voltage source, R is the resistance of the circuit, i is the current passing through the circuit and L is the non-linear inductance of the solenoid that is dependent on the air gap, between the fixed magnetic core and the mobile magnet, and on the current.

If a simple model of the coil with a resistance, an inductance and a power supply is considered, where eddy currents are still ignored and where the inductance is considered constant, we can have:

$$V = iR + L \frac{di}{dt} \quad (2.2)$$

The solution of which with respect to current $i(t)$ is:

$$i(t) = \frac{V}{R} (1 - e^{-\frac{t}{\tau}}) \quad (2.3)$$

Where current has been expressed as a function of a time constant $\tau = \frac{L}{R}$. From this equation can be seen that the electric response is strongly dependent from the inductance, furthermore the time response is also inhibited by the eddy current, the effect of which is pretty strong for small air gaps.

2.4.3 Inductance Analysis

As the plunger moves, the air gap and the density of the magnetic flux lines will change, affecting the magnetic field inside the magnetic circuit. Moreover a movement of the plunger will also result in a change in the inductance. So, from the simplification of the expression of the inductance as a linear function of the plunger's position x, can be obtained:

$$L(x) = L_{x_1} + \frac{L_{x_1} - L_{x_2}}{x_2 - x_1} x \quad (2.4)$$

Where L_{x_1} and L_{x_2} are respectively the inductance for both maximum and minimum air gaps, x_2 and x_1 are the position of the plunger at the maximum and minimum air gaps and x is the actual position of the plunger.

From a comparison between the two values of inductance at the extremes of the plunger's stroke, which correspond an air gap of 0.4mm and 0.625mm respectively, has been seen that the variation of inductance is so small that can be neglected and assumed constant. So, from the classic formula, for the coil it can be computed as:

$$L = \frac{\mu_0 A N^2}{l} i \quad (2.5)$$

Where μ_0 is the vacuum permeability, A is the section area of the solenoid, N are the number of turns of the wire around the solenoid and l is the length of the solenoid. The previous value of inductance is valid for the nude circuit, but in our case the solenoid wraps a ferromagnetic material, this will be seen in detail in the next paragraph. We must correct the value of the inductance substituting the vacuum permeability with the relative permeability μ_r of the material in order to obtain:

$$L = \frac{\mu_r A N^2}{l} i \quad (2.6)$$

2.5 Magnetic Model

In this section the behavior of the magnetic parts of the valve have been described. First of all a rough analysis has been done considering constant all the section of the magnetic circuit. So the geometry and the relations between magnets have been clarified and the magnetic part's equations have been described. Then, a second order and more precise analysis has been done considering the section variation of the magnetic circuit.

2.5.1 Magnetic Circuit

The geometry of the valve can be seen in the following figure.

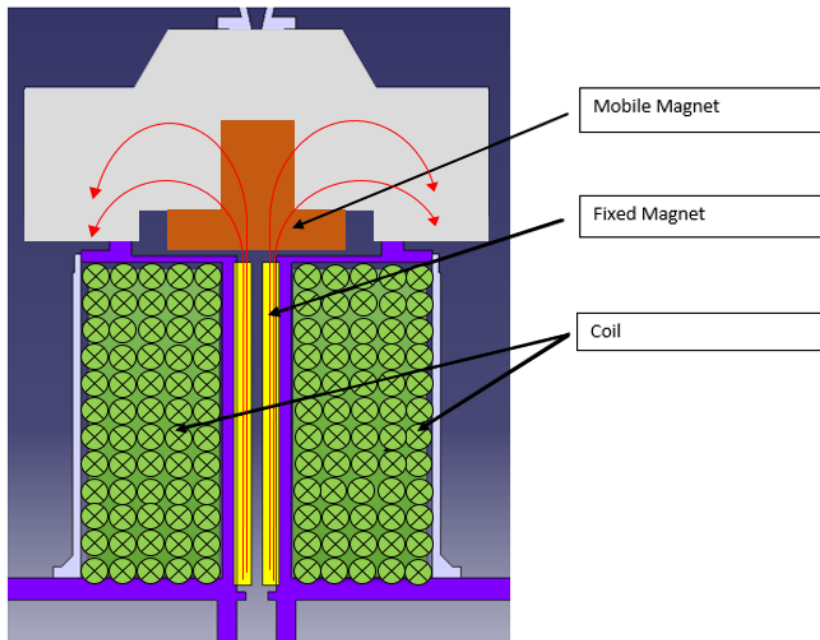


Figure 2.4: Valve Section

Our solenoid actuator consists of a static part formed by the coil and the fixed magnet, or namely, ferromagnetic core. The dynamic part is composed by the mobile magnet which is attached to the plunger. When the current is applied to the coil, a magnetic field is generated and the electromagnetic energy is stored in the field. Consequently, a magnetic force is exerted

between the ferromagnetic core and mobile magnet allowing the movement of the second towards the first one.

The magnets are fabricated from a soft ferromagnetic material named "Vacoflux". Its characteristic magnetization curve is reported in figure 2.5

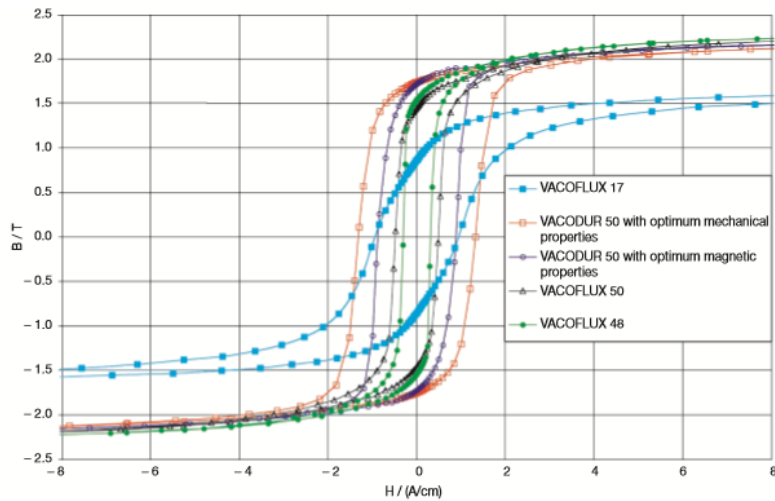


Figure 2.5: Vacoflux Magnetization Curve

It has to be underlined that these are typical loops for strips with a thickness of 0.35 mm, anyway momentarily we just need to know that its properties as soft magnet allow us to treat our actuator as an electromagnet. In other words, our magnetic field is generated only when we close the electric circuit, in fact the residual flux density B_r is typically low in these materials and can be neglected. Another important property regard the relative permeability μ_r of ferromagnetic materials, it is a dimensionless number which increase the vacuum permeability μ_0 of several order of magnitude and it depends by position inside the material and by the direction of the magnetic flux lines. Regardless, being our material homogeneous and isotropic, its behavior is considered linear.

It has to be noted that the analytic expression of the magnetic force is very complex for this experimental prototype. Then, the magnetic force characteristics are experimentally calibrated as a function of the applied current

and the plunger position.

2.5.2 Magnetic Equations

From the magnetic circuit scheme of figure 2.5, using the Ampere's theorem the equation of the magnetic circuit can be expressed as:

$$l_{gap} H_0 + l_{circ} H = Ni \quad (2.7)$$

Where l_{gap} and l_{circ} represent respectively the length of the air gap and of the magnetic circuit, H_0 and H are the magnetic field intensity in the air gap and in the material, N represent the number of turn of the wire in the solenoid.

From literature we know that the magnetic flux φ in a magnetic circuit is constant during all the length of the circuit. Using the assumption that our magnetic circuit has a constant section, the relation between the field intensity H and the magnetic flux density B is given by:

$$B = \mu_0 H_0 = \mu_r H_i \quad (2.8)$$

Where $\mu_r = k_r \mu_0$ in which k_r is a constant of the material.

Substituting, it can be obtained the magnetic flux density B written as:

$$B = \frac{k_r \mu_0 N i}{k_r l_{gap} + l_{circ}} \quad (2.9)$$

Making the comparison between the terms at the denominator of the previous expression can be noted, from the geometry of the circuit and the properties of the material, that:

$$\frac{k_r l_{gap}}{l_{circ}} \approx 10^2 \quad (2.10)$$

So we can simplified equation writing:

$$B \approx \frac{\mu_0 Ni}{l_{gap}} \quad (2.11)$$

Finally we can express the magnetic force as:

$$F_m = \frac{\varphi^2(i)}{2\mu_0 A} = \frac{A}{2\mu_0} \left(\frac{k_r \mu_0 N i}{k_r l_{gap} + l_{circ}} \right)^2 \approx \frac{\mu_0 A (N i)^2}{2 l_{gap}^2} \quad (2.12)$$

Where φ is the magnetic flux passing through the coil. Note that l_{gap} can be written as function of the position of the plunger. We have to remember that this equation is valid only with the assumption of a constant section for our magnetic field.

2.5.3 Second Order Analysis

In order to have a better idea regard the force exerted between the magnets for different air gaps we have to go deeper into the study of our magnetic circuit. The computation has been done using the software *MatlabTM* and the code is reported in the appendix.

The reluctance of an element in a magnetic circuit is given by:

$$\mathfrak{R} = \frac{l}{\mu_r A} \quad (2.13)$$

As we can see in the following image, the section A along its length l is not constant. We can assume the reluctance of this part as the sum in series of two different parts of the magnetic circuit.

So equivalent reluctance can be written as:

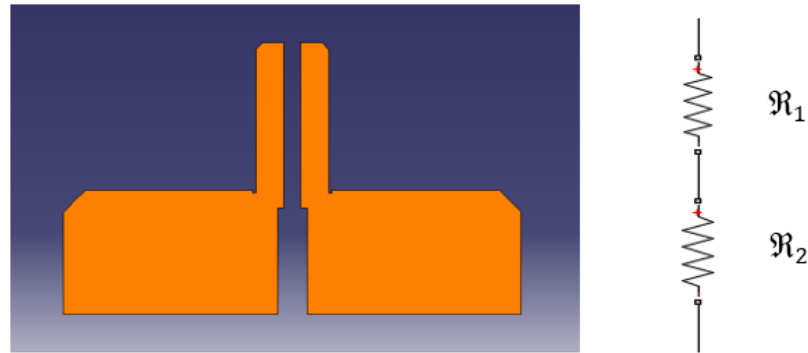


Figure 2.6: Movable Magnet Section

$$\mathfrak{R}_{eq} = \mathfrak{R}_1 + \mathfrak{R}_2 \quad (2.14)$$

It is now possible imagine an analogy between the magnetic circuits and the electric ones. So in the electric circuit the difference in voltage V produces a current i and all is contrasted by the resistance R , as in our magnetic circuit the current in the solenoid Ni produces a magnetic flux φ that is opposed or enhanced by the reluctance \mathfrak{R} .

Therefore we can build up our magnetic circuit as:

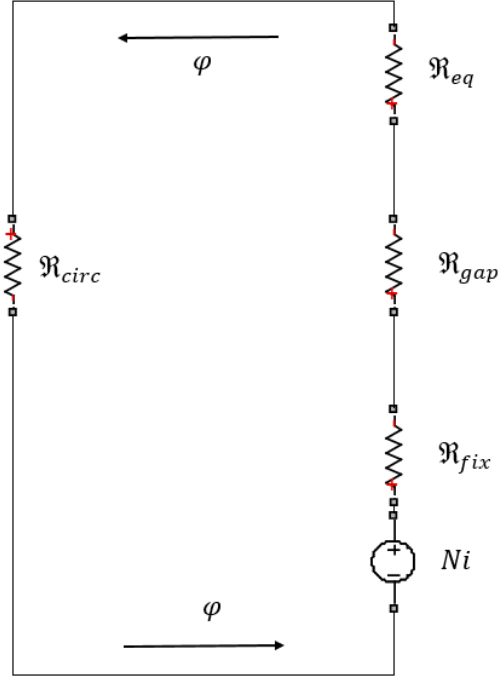


Figure 2.7: Detailed Magnetic Circuit

Where Ni is the magneto motive force, \Re_{fix} is the reluctance of the fixed magnet, \Re_{gap} is the reluctance of the air gap, \Re_{eq} is the reluctance of the movable magnet as computed before, \Re_{circ} is the reluctance of the rest of the circuit and φ is the magnetic flux.

Now all the reluctance \Re of the various parts of the circuit have been considered. So we can write the total reluctance of the circuit as:

$$\Re_{tot} = \Re_{fix} + \Re_{gap} + \Re_{eq} + \Re_{circ} \quad (2.15)$$

The magnetic flux passing through the circuit can be computed as:

$$\varphi = \frac{Ni}{\Re_{tot}} \quad (2.16)$$

From this we can compute the magnetic flux density in every parts of the circuit from:

$$B_j = \frac{\varphi}{A_j} \quad (2.17)$$

Where j represent the various parts of different length and section of the circuit.

And the magnetic field intensity is given by:

$$H_j = \frac{B_j}{\mu_0 \mu_j} \quad (2.18)$$

Finally the magnetic force can be computed as:

$$F_{mag} = \frac{\partial U_{mag}}{\partial x} = \frac{(Ni)^2}{2} \frac{\partial}{\partial x} \left(\frac{1}{\mathfrak{R}} \right) = -\frac{(Ni)^2}{2\mathfrak{R}^2} \frac{\partial \mathfrak{R}}{\partial x} \quad (2.19)$$

So in cases of maximum (0.625 mm) and minimum (0.4 mm) air gap between the magnets, we have:

$$F_{mag_{max}} = -\frac{\mu_0 A_0}{2} \left(\frac{Ni}{l_{max}} \right)^2 \quad (2.20)$$

$$F_{mag_{min}} = -\frac{\mu_0 A_0}{2} \left(\frac{Ni}{l_{min}} \right)^2 \quad (2.21)$$

2.6 Mechanical Model

In order to understand the behavior of the plunger we can do a balance between the forces that act on it. Neglecting the viscous forces between the plunger and its rail and also avoiding the viscous force due to the gas, the equilibrium equation of the plunger is composed by:

- The magnetic force acting on the mobile magnet F_m ;
- The force of the spring F_k ;
- The force of the gas F_{gas} .

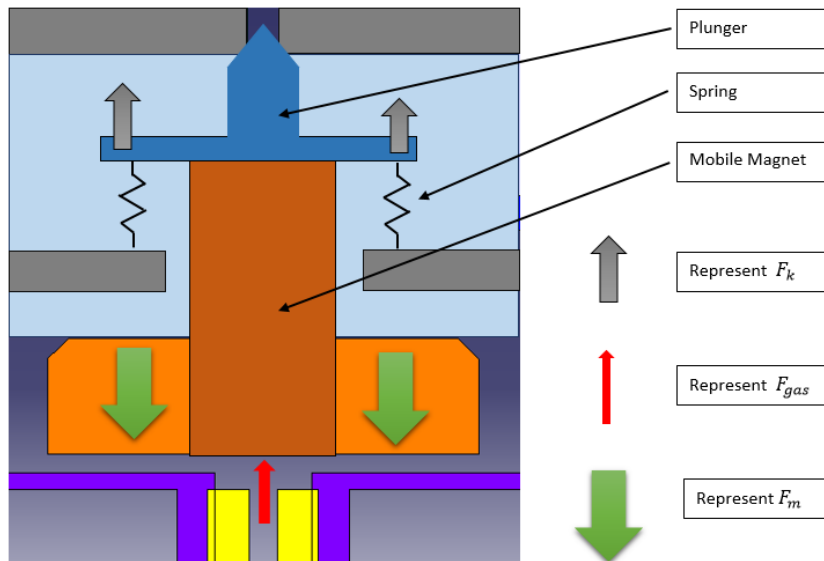


Figure 2.8: Forces Equilibrium Scheme

The force of the spring can be written as:

$$F_k = k(x + l_0) \quad (2.22)$$

Where k is the spring constant, l_0 is the length of the pre-load and x is the position of the plunger. Note that this force always acts to close the valve with different magnitude depending on the operating point of the valve.

Approximating the force of the gas as hydrostatic pressure I can write:

$$F_{gas} = pS_{eq}F_{gas} = pS_{eq} \quad (2.23)$$

Where p is the pressure of the gas acting on the plunger and S_{eq} is the equivalent section of the plunger affected by the pressure p . The dynamics of the gas will be examined in the next section, anyway we can immediately note that as long as the pressure of the environment that surround the valve is zero, like in vacuum, this force acts only to close the valve. Therefore we can see that the only force that operate to open the valve is the magnetic force.

Looking at the system shown in figure 2.8, considering the assumptions done and basing on Newton's second law, the dynamic motion equation of the plunger can be written as:

$$m\frac{d^2x}{dt^2} + kx = F_m(i, x) + F_{gas} + F_{k0} \quad (2.24)$$

Where m is the mass of the movable part of the valve and F_{k0} is the pre-load force of the spring.

2.7 Hydrodynamics Model

The fluid dynamic model is used to describe heat transfer and the dynamics relations of the gas which passes through the valve. In this analysis, the Xenon propellant has been considered as gas and it has been assumed ideal in this model. Furthermore the heat due to compression or expansion is minimal, in first approximation, and it has also been neglected with the comprimibility of the fluid.

Using the law for perfect gas, the pressure in the valve can be expressed as:

$$p = \frac{m\mathcal{R}T}{M_{Xe}V} \quad (2.25)$$

Where p is the pressure, m is the mass of the gas, \mathcal{R} is the universal gas constant, T is the temperature of the gas in the valve, M_{Xe} is the molecular weight of Xenon and V is the volume of the gas in the valve.

Differentiating the previous expression I obtain:

$$\dot{p} = \frac{\mathcal{R}T}{M_{Xe}V}\dot{m} + \underbrace{\frac{m\mathcal{R}}{M_{Xe}V}\dot{T}}_{\approx 0} + \underbrace{\frac{m\mathcal{R}T}{M_{Xe}V^2}\dot{V}}_{\approx 0} \quad (2.26)$$

Where the changes in temperature and volume are neglected.

Furthermore the external pressure can be considered negligible, so the assumption of chocked flow can be done. Doing this, the mass flow rate for our valve has been assumed as maximum and it can be expressed as:

$$\dot{m} = \frac{pA\gamma}{\sqrt{\gamma\mathcal{R}T}} \left(\frac{2}{\gamma+1} \right)^{\frac{\gamma+1}{2(\gamma-1)}} \quad (2.27)$$

Where γ is the specific heat ratio of the Xenon and A is the minimum area of the fluid's leakage.

The mass flow of the gas depends on the plunger's position. If the plunger is in contact with the stopper, no gas can flow through the valve. As soon as the plunger moves, the area of fluid's leakage get bigger and the mass flow rate increase according the previous relation. When the leakage area became equal to the outlet area of the orifice the mass flow rate stops to rise. The orifice's area is constant, and can be expressed by:

$$A_0 = \frac{D_0^2}{4} \quad (2.28)$$

Where D_0 is the diameter of the orifice (0,3 mm).

In order to understand how the leakage area is influenced by the position of the plunger can be helpful a comparison between the lateral area of the frustum and the area of the orifice. It has been reported in figure 2.9 a scheme of mechanism that allows the passage of the fluid through the valve.

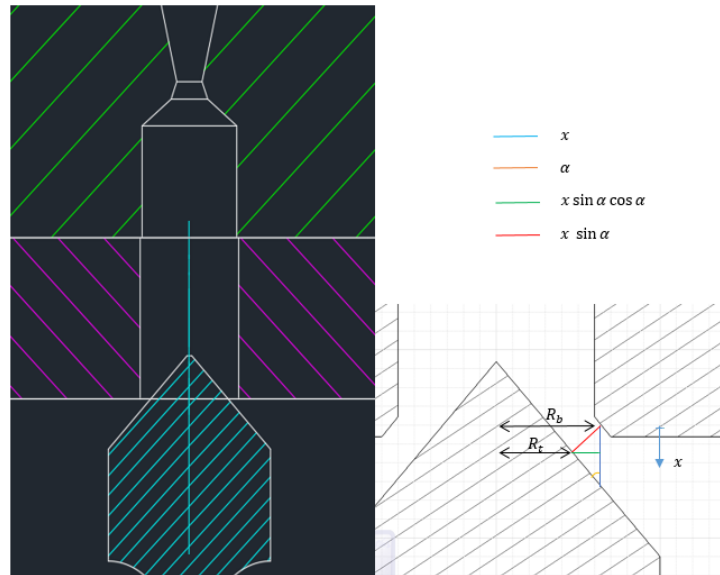


Figure 2.9: Geometry Analysis of the Seal mechanism

From figure 2.6 we can realize that mass flow depends on the surface area of the frustum created by the relative position of the plunger and the stopper. This area can be computed using:

$$S_l = \pi \left[R_b + \underbrace{(R_b - x \sin \alpha \cos \alpha)}_{R_t} \right] \underbrace{x \sin \alpha}_{a} \quad (2.29)$$

Where R_b is the base radius of the frustum, R_t is the tip radius, α is the angle of inclination of the straight line generating the cone of the plunger, a is the apothem of the frustum and x is the position of the plunger.

It is now possible making a comparison between the area of the orifice A_0 and the lateral surface of the frustum S_l . Doing this we see that for almost one fourth of plunger's stroke ($x = 0,056$ mm), the lateral surface of the frustum is almost the double of the area of the orifice. So we can assume that when the valve is open, the limit of the outlet orifice's area is immediately reached, therefore the mass flow of the gas is independent from the position of the plunger. This is quite relevant for our study because allow us to decouple the equilibrium equation from the fluid dynamic relation.

2.8 Heating Equations

In this section the code used to compute the overheating of the coil for different configurations. And in this case, unlike the previous codes, the equations has not been reported in chapter 2 so we must present them.

From the 3rd Ohm's law can be easily obtained the following relation:

$$P = i^2 R(T) \quad (2.30)$$

So the energy can be obtained by integer:

$$E(t) = \int P dt = \int i^2 R(T) dt = i^2 R(T) \Delta t \quad (2.31)$$

From the energy equation for a copper wire supplied by electrical current we have:

$$E(t) = c_{cu} m \int_{T_i}^{T_f} dT = c_{cu} m \Delta T \quad (2.32)$$

where c_{cu} is the specific heat of Copper and m is the mass of the wire.

Rearranging we can compute the time interval to reach the final temperature as:

$$\Delta t = \frac{c_{cu} m \Delta T}{i^2 R(T)} \quad (2.33)$$

The situation represented by this equation is the adiabatic case, without any exchange of heat with the environment. Obviously, this approximation has been used to overestimate the effect of the temperature on the coil, in fact have not been considered several effect such as the radiation and the conduction of the coil. The previous formula has been used to compute the time interval in order to have a certain variation of temperature, in our case

this variation is between the initial temperature of the coil and the its fusion temperature.

Another clarification that has to be done regard the term of resistance $R(T)$ and its dependence by the temperature. For a Copper wire the resistance is given by:

$$R(T) = \frac{4\rho_{cu}(T)l_w}{\pi D_w^2} \quad (2.34)$$

where ρ_{cu} is the Copper electric resistivity, l_w is the length of the wire and D_w is its diameter. The Copper electric resistivity is given by the following empirical formula:

$$\rho(T) = 1,56(1 + 0.00438 \cdot T) \cdot 10^{-8} \quad (2.35)$$

where the temperature T has to be insert in Celsius.

2.9 Model Summary

In this section the equations for the complete model are collected.

$$\left\{ \begin{array}{l} \frac{di}{dt} = \frac{V - Ri}{L_{x_1} + \frac{L_{x_1} - L_{x_2}}{x_2 - x_1} x} \\ \frac{d^2x}{dt^2} = \frac{\mu_0 A(Ni)^2}{2mx^2} + \frac{pS_{eq}}{m} + \frac{k}{m}(x + l_0) \\ \frac{dp}{dt} = \frac{\mathcal{R}T}{\mathcal{M}_{Xe}V} \frac{pA\gamma}{\sqrt{\gamma\mathcal{R}T}} \left(\frac{2}{\gamma+1} \right)^{\frac{\gamma+1}{2(\gamma-1)}} \\ \frac{dT}{dt} = \frac{i^2 4 \rho_{cu} l_w}{c_{cu} m \pi D_w^2} \end{array} \right. \quad (2.36)$$

For the sake of simplification we can rewrite and discretize the system as:

$$\left\{ \begin{array}{l} \frac{di}{dt} = -\frac{R}{L}i + \frac{V}{L} \\ \frac{d^2x}{dt^2} = \frac{\mu_0 A(Ni)^2}{2mx^2} + \frac{pS_{eq}}{m} + \frac{k}{m}(x + l_0) \\ \frac{dp}{dt} = \frac{\mathcal{R}T}{\mathcal{M}_{Xe}V} \frac{pA\gamma}{\sqrt{\gamma\mathcal{R}T}} \left(\frac{2}{\gamma+1} \right)^{\frac{\gamma+1}{2(\gamma-1)}} \\ \frac{dT}{dt} = \frac{i^2 R}{c_{cu} m} \end{array} \right. \quad (2.37)$$

This system is composed by three first order linear differential equations and by one second order non linear differential equation.

Chapter 3

Valve Optimization

In this chapter have been shown the modifications done on the various valve's parts. Firstly the main assumptions and the approach to this problem have been explained. Then a list of the modified parts has been presented. Each part has been compared with the previous version in order to better show the changes generated. Finally some hypothesis for the future modification and implementation have been made.

3.1 Design Approach

In this section the approach to the valve's modifications has been explained. Starting from the analysis of the first version components of the valve it has been decided to modify only on the external parts and the coil of the valve, to not distort the basic principles of valve's work. From these initial assumptions has been possible to identify the pieces to modify. So the dimensions of these pieces have been reduced and a model for the coil computation has been developed using the software *MatlabTM*. The materials of the various parts, so as their characteristic shape, have not been changed. Then, when it has been necessary, a new mechanism of junction has been created. It must be underlined that the modifications have been done with the aim to alter as less as possible the shape of the valve.

3.2 Spring Modifications

The spring is one of the main component of our system because the closure and the tightness of our valve depend directly from it. In our case, the spring is a plane spiral one made of Titanium alloy.

In order to not compromise its functional aim or its mechanical characteristics, the possibilities to produce some changes were very restricted. In fact, both external and internal diameters, the thickness and the basic shape have not been modified. Have been changed only the extremities of the spiral extrusions, by the way we can appreciated the benefits of this operation through the following figures.

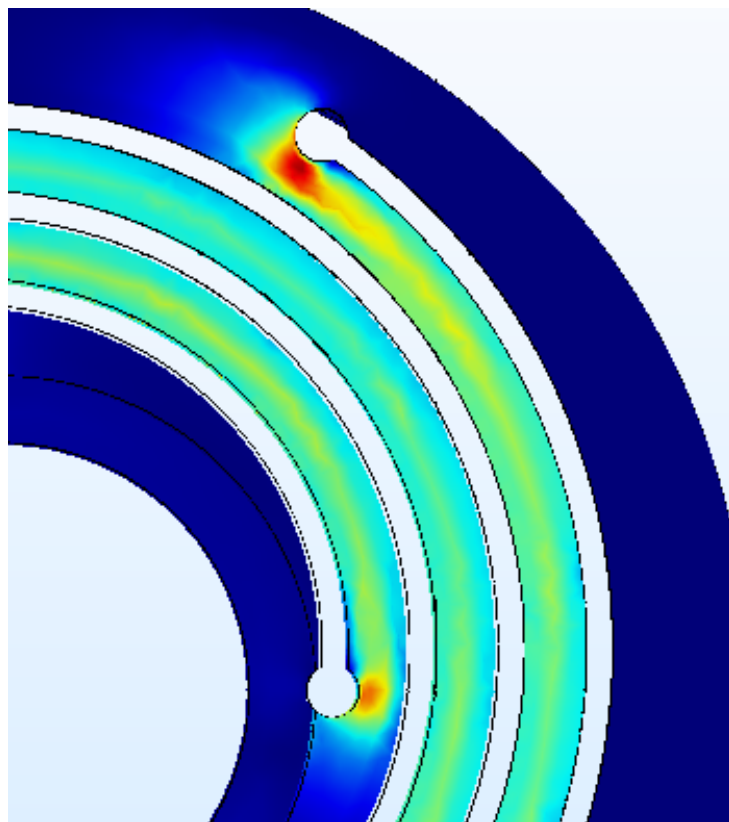


Figure 3.1: First Version Spring

From figure 3.1 can be easily noted that the stresses are concentrated among two particular points of the spring. In order to avoid such intensifi-

cation of the stresses and to guarantee a better and longer use of the spring, several simulations have been done. The modified shape is represented in the figure 3.2.

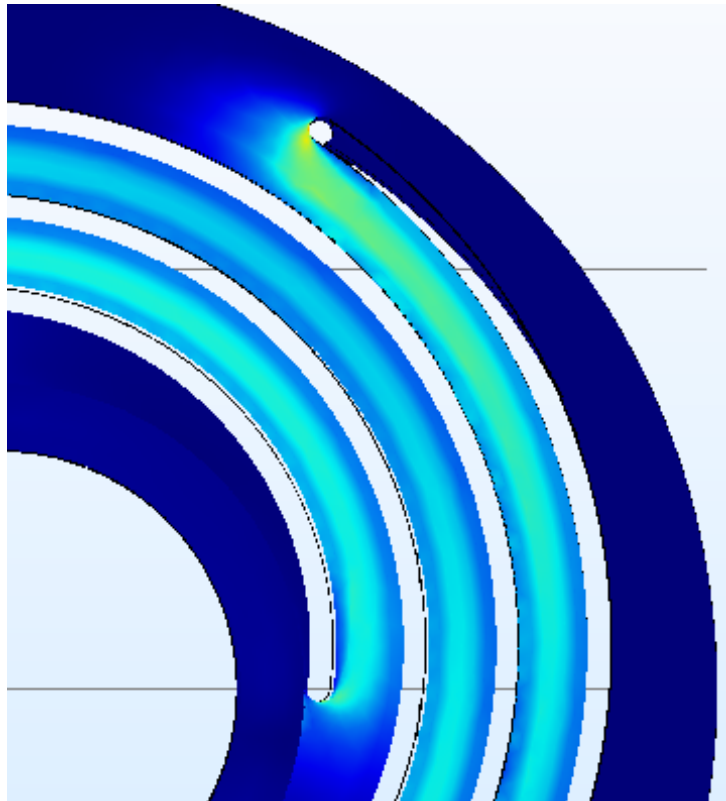


Figure 3.2: Modified Spring

As can be seen, the stresses are distributed more homogeneously among all the spring's structure, furthermore its basic shape is practically untouched. Another element of relevance is the reduction of the number of operations needed to make the new spring. It has to be underlined that the spring has to be tested to fatigue before the implementation in the valve, even if usually the valves used for this application don't have to guarantee an high number of cycles.

3.3 Coil Case Modifications

The Coil Case is the part used to cover and protect the coil from external disturbances or damages. It can be composed by a single piece of Aluminum alloy or, as in our case, it can be formed by two complementary and symmetric pieces in order to render the feasibility and manufacturing more allowable. It does not affect the structure resistance of the valve but it interacts directly with the magnetic flux generated by the coil, so the choice of the material has a relative importance for this part.

In order to guarantee its functionality its dimensions have been changed with the dimensions of the coil. Differently from the spring, heavier modifications have been done on this piece because of its smaller functional importance. The main differences can be identified by the following figures.

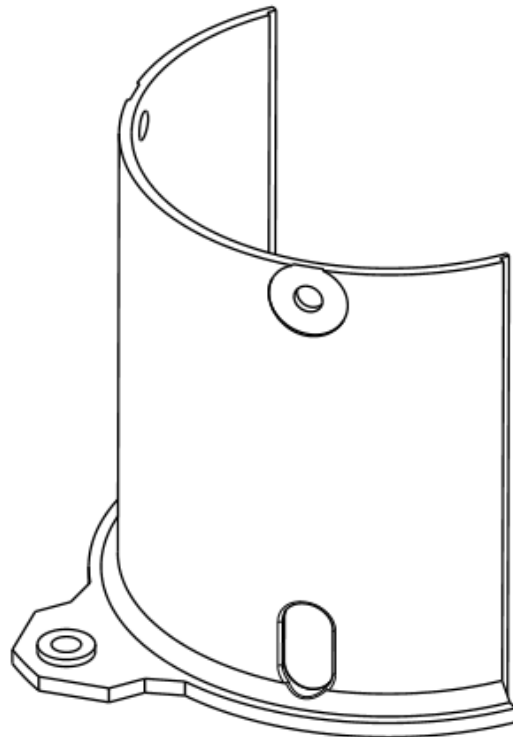


Figure 3.3: First Version Coil Case

From figure 3.3 can be easily seen the symmetric shape of this part, moreover can be noted that the lower part is quite bulky, this has been necessary to guarantee the attachment the the rest of the valve.

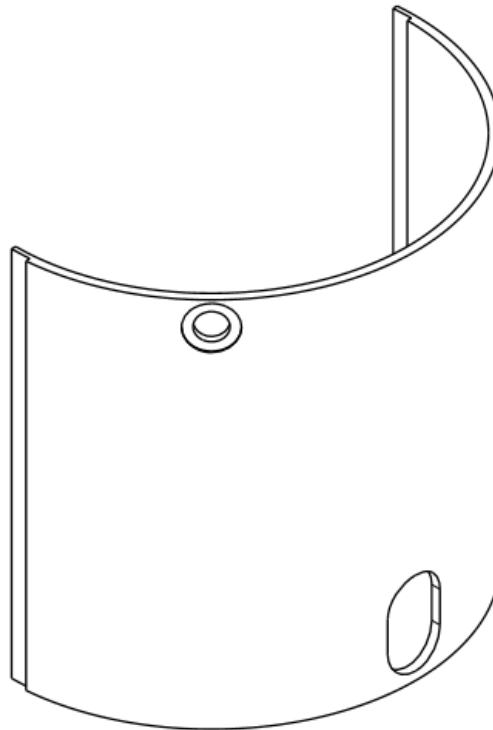


Figure 3.4: Modified Coil Case

The figure 3.4 represents the modified version of the Coil Case. Its lower part has been shrunk, anyway the attachment to the rest of the valve has been ensured by a modification that is going to be illustrated in the next section. Furthermore also the thickness of the semi-cylindrical part has been reduced.

3.4 Main Case Modifications

The Main Case is the base structural part of the valve and its functions are multiple. It has to guarantee the mechanic resistance in any possible scenario, it also has the task to connect the valve to its support. In its central part is wrapped the the Copper wire, so it hold up the coil. Finally in its inner parts there is located the ferromagnetic core which covers a crucial role for the functionality of the mechanism.

The importance of this piece is easily understandable, so in order to not create alterations or malfunctions of the mechanism only the external and the upper part are been changed. We can observe these modifications in the following figures.

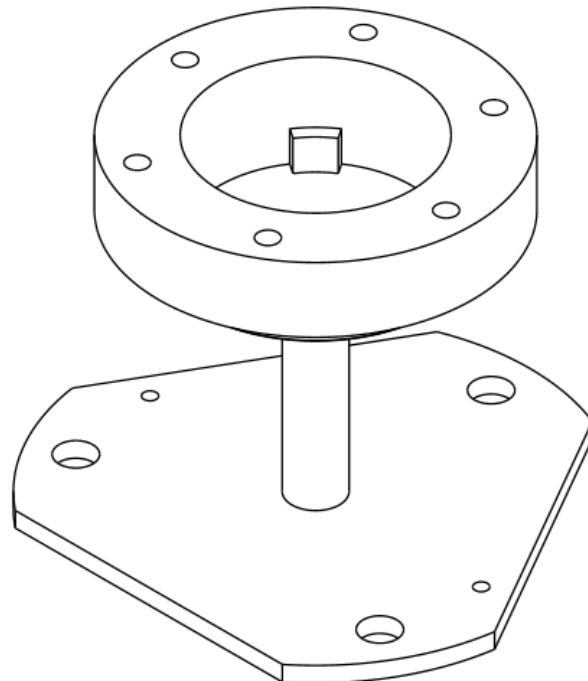


Figure 3.5: First Version Main Case

From figure 3.5 can be noted the large base compatible with the first version of the Coil Case, the piece analyzed before. Furthermore we can see that in the upper part there are located six holes which occupy a great portion of the cross area.

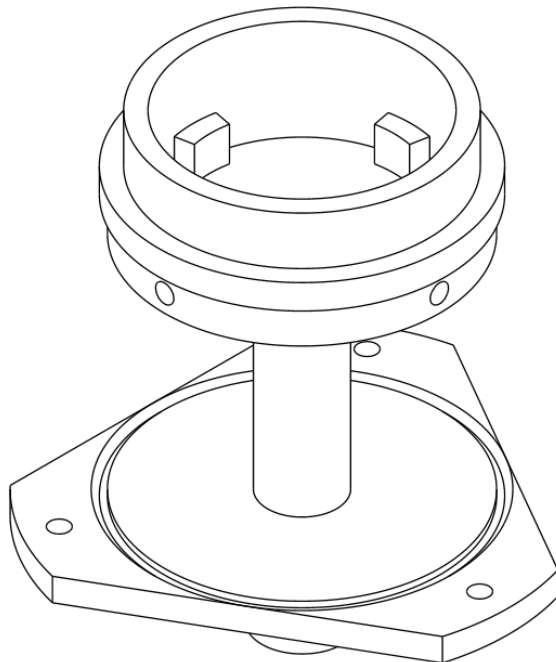


Figure 3.6: Modified Main Case

Figure 3.6 represents the modified version of the Main Case, we have to underline that the diameter of the cylinder that connects the lower part to the upper one has not been changed, so we can better appreciate the order of magnitude of the dimensions reduction of the entire piece. The base has been shrunk and modified in order to support the modified Coil Case. The upper part can be now screwed in the Main Body Front, which is going to be analyzed in the next section, consequently it allows us to save some space from the removal of the six holes present before.

3.5 Main Body Front Case Modifications

The Main Body Front Case is the upper part of the external shell of the valve. It contains the mobile apparatus of the mechanism. For this reason the inner part of this piece has been modified the less as possible, however the external dimensions have been reduced and its configuration changed.

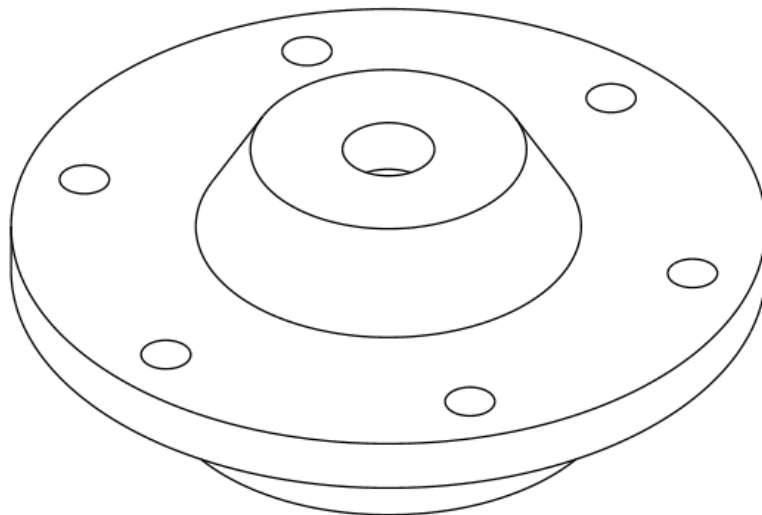


Figure 3.7: First Version Main Body Front Case

As we can see from figure 3.7 a large portion of space is occupied by the external ring in which there are located the six holes which aim is to connect this piece to the previous one. In order to shrink this component, it is arranged as in the next figure.

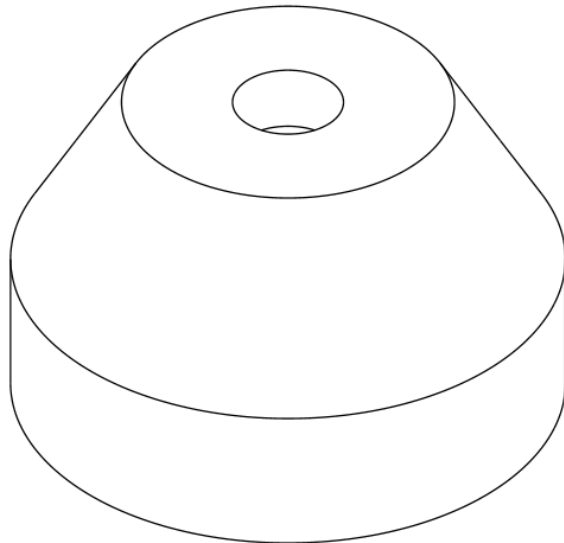


Figure 3.8: Modified Main Body Front Case

Figure 3.8 represent the modified version of the Main Body Front Case, we can immediately note that the external ring has been neglected, nevertheless the mechanism of junction has not been forgotten. In fact the inner part of this new piece has been designed in order to screw on the Main Case analyzed before. This mechanism could create problems of tightness between the two pieces, so it has been thought to use a Microring to fix them.

3.5.1 Micro O-ring Implementation

As a general definition, a MicrOring seal is any O-ring that measures less than 1 mm in either inside diameter or cross section. MicrOring seals were developed to meet the ever-increasing demand for effective seals in a wide range of miniaturized applications, from precision instruments and medical devices to aerospace and fiber optics.

In sealing applications, correct O-ring selection is the result of a number of design considerations including dimensions, chemical compatibility, and the material physical properties to resist pressure and temperature extremes. It has to be underlined that the component dimensions and tolerances become more important as the O-ring size gets smaller. A list of some basic sealing concepts has been presented:

- **Sealing force**, it is the normal force exerted by the resiliency of the elastomeric seal when squeezed between the mating surfaces of the gland geometry. The sealing force increases as the system pressure is transmitted through the seal geometry.
- **Low pressure sealing**, the system pressure is low, so the design must rely on the resilience of the elastomer to retain the needed sealing force. A proper seal material selection and surface finish are critical to have an effective seal.
- **High pressure sealing**, the system pressure is high, so particular attention has to be given to seal material hardness and hardware clearances to prevent potential seal extrusion.
- **Tolerance stack up**, it is an especially important factor in micro-miniature O-rings due to the fact that the tolerances account for a large percentage of the nominal O-ring size. In a sealing application, the tolerances of all the parts in contact with the O-ring must be considered in order to create an effective seal. The combination of these tolerances is the tolerance stack-up.

In order to avoid various problems related to structural resistance of the main body front, the part which holds the microring's seal, and others problems related to interference with the assembly of the valve, two positions could be selected for the positioning of the microring. Then, in order to positioning the microring as far as possible from a zone probably subjected to welding, the final position has been found. The dimension has been chosen

in order to have the best compromise between the structural resistance of the main body front and the seal of the bond. For these reasons the microring has been chosen by the catalog of an United Kingdom company named Apple Rubber, a part of the catalogue is reported in the following figure:

INCHES		MILLIMETERS	
Inside Diameter	Cross Section	Inside Diameter	Cross Section
0.776	0.031	19.71	0.79
0.776	0.032	19.71	0.81
0.776	0.039	19.71	1.00
0.779	0.031	19.79	0.79
0.780	0.024	19.81	0.61
0.780	0.031	19.81	0.79
0.780	0.039	19.81	1.00
0.785	0.030	19.94	1.00
0.787	0.024	20.00	0.61
0.787	0.030	20.00	0.76

Figure 3.9: MicOring Table

As indicated by the selection in red, the microring has an inner diameter of 20 mm and a cross section of 0,61mm, which allow us to put it in a gland deep 0,6 mm avoiding a compression superior at the 6% of its cross section.

Finally a quick study about the materials available has been done. It has been preferred a fluorosilicone oring to a classical buna-N oring because of its major resistance to both high and low temperatures. In fact these orings can stand in a range from -60° C to 200° C against the -40° C to 125° C range of the common buna-N.

3.6 Assembly Comparison

In this section, a comparison between the two versions of the valve has been showed in order to put in evidence the differences between the two configurations. As said yet, only the external part of the valve has been modified and with respect to the agreement took with Aerospazio Tecnologie s.r.l. only an outlook view of the valve can be reported. The measures have been reported in millimeters.

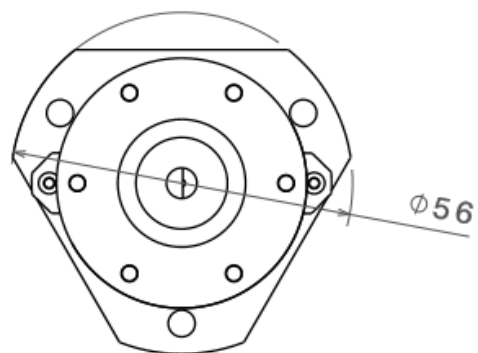
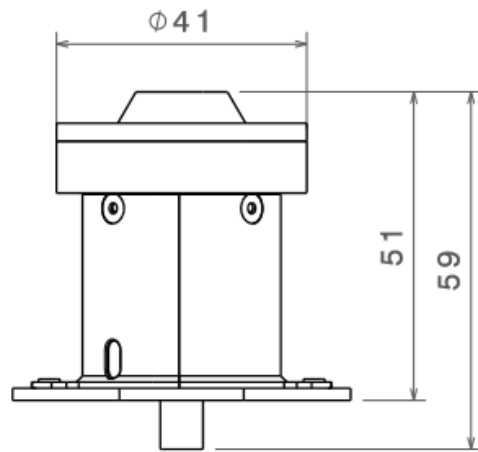


Figure 3.10: First Version Dimensions

Figures 3.10 and 3.11 show us the new version of the valve, it has been reduced in height of 9mm and in width of 16mm, which correspond to a shrink respectively of the 18% and 39%.

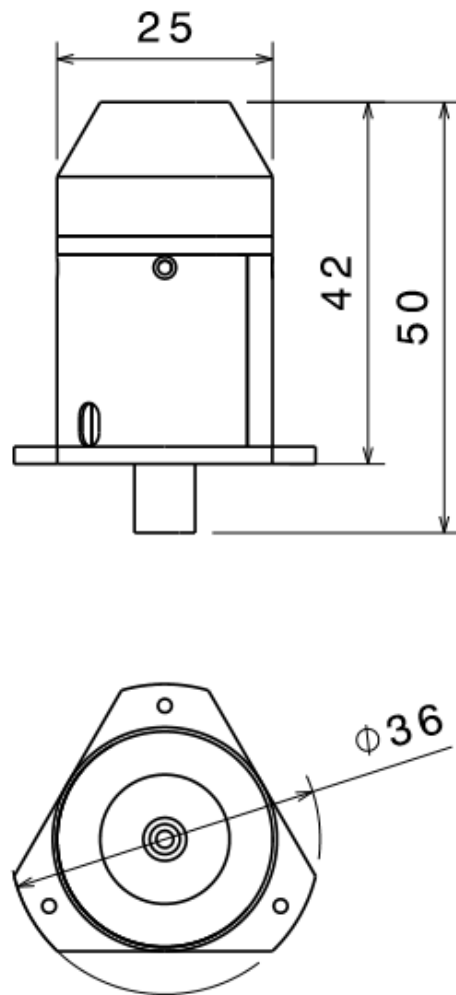


Figure 3.11: Modified Version Dimensions

It has to be remembered that this configuration represents the first modified version of the valve, then its dimensions could be reduced further in future.

3.7 Coil Modifications

The Coil is an active component of our system and it allows us to change the operative state of our system passing through it an adequate current flow. It consists in a Copper wire of a certain diameter and length wrap around a ferromagnetic material. Obviously, the number of turns of the coil depends on the geometry and on the performance needed, its dimensions are strictly related to the ones of the case. Usually it also represents the major amount of space of a solenoid valve, for this reason it has been decided that the greater modifications had to be done around it. Furthermore the design of a coil has a great amount of literature to take as starting point.

As material of the Coil has been used a classic enameled Copper wire because of its availability on the market and consequently its low cost. However other types of material have been tested with inefficient results, so the Copper has been selected as the best compromise between performances and costs.

The configuration of the Coil has been selected as a multi-layer one. This choice has been forced by the necessity to shrink at minimum the space occupied by the Coil Case, furthermore in a single-layer configuration the valve would have appeared too much tapered. During the computation, the coil radius has been considered the average radius of the multi-layer wrapping.

The choice of the numbers of turn and the wire diameter was of relevant importance for our valve. In order to make the best decisions for our aim, different models of the coil have been created using the software *MatlabTM*. The *MatlabTM* codes have been reported in the appendix and the work done on it has been explained in the following chapter.

Because of the versatility of this type of valve when the volume occupied is reduced to minimum, the response time could not fulfill the request of various applications. In order to avoid these problems a pick and hold strategy has been studied.

3.7.1 Pick and Hold Strategy

This strategy has been thought to be used in the case of our valve has to be used as a Cold Gas Thruster. The utilization of these systems usually required the exit of a gas flow rate as a series of impulses in a small period of time.

The peak and hold drive circuit applies a higher current to the solenoid while it is at its open or maximum air gap condition. Once the solenoid has completed its travel to the closed or minimum air gap position, the current is reduced to the hold current level, which maintains the solenoid in this position until the current is removed. The current amplitude and time duration of the peak and hold drive signals are application dependent and are modified to match a given application. The characteristic input signal and output current are reported in the figure below.

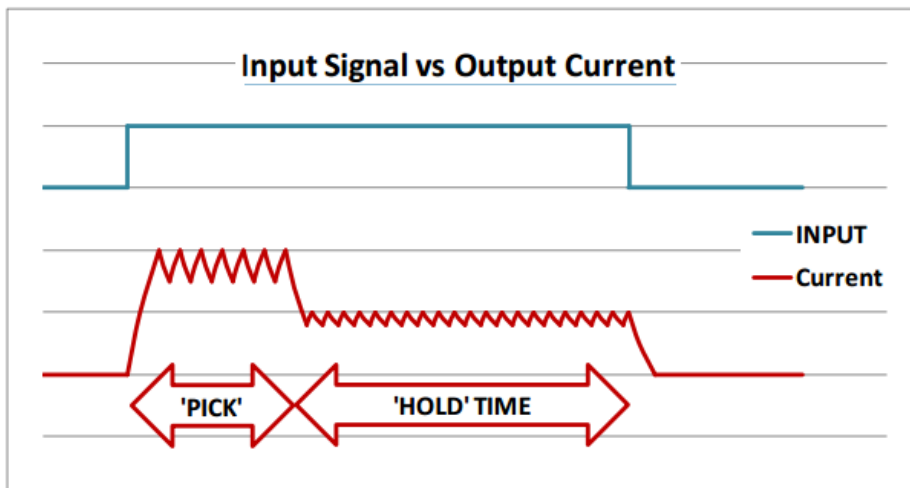


Figure 3.12: Pick and Hold Graph

Obviously different parameters as both the pick and hold amplitude or duration can be computed and optimized. However these evaluations have been left for a later and deeper study.

Chapter 4

Simulations and Models

In this chapter v It has been created using the software *MatlabTM*. Firstly the approach to the problem is showed, then the main parts of the code are described and finally two complete simulations are reported in order to put in evidence their differences.

4.1 Procedure of Development

Initially a first order model for each relevant aspect of the valve has been done. In these phase the main problems has been given by the absence of some experimental data and initial parameters, so in order to get closer as possible to the real cases, some of these missing data have been taken from literature. A brief list of these short models are presented in the next section.

Then these codes have been implemented in just one main code in order to make a comparison between the data collected by every code and verify their reliability. This verification has been done by comparison with the data founded in literature.

Now one of the initial parameter of the has been inserted into the code as a vector in order to collect different results with the different values of this parameter. The diameter of the enameled Copper wire has been chosen as

crucial parameters, in fact if our task is the shrinking and the optimization of the valve, there's no parameters that affect on the reduction of the space occupied more than the diameter of the wire. We have to underline that in the first version of this valve the copper coil occupies almost the 50% of the total volume of the valve.

Finally from the main code other two codes have been derived in order to better define the parameters of our valve. In one code the Ampere-Spire has been kept constant, this gave us the opportunity to see the changes in time to fusion and in power requirements for the different configurations and to define the minimum electromagnetic strength exhortated by the valve. In the second code the Power has been kept constant, this show us the variation of the electromagnetic strength with the diameter of the wire and the number of spire. Doing this, various configurations have been simulated and the best two have been chosen.

4.2 First Order Codes

In this section the main code parts are presented and the result showed. In order to avoid the repetition of the 2nd chapter's equations in this section has not been reported the equations used but just their results and formulation.

4.2.1 Electric Code

This code has been developed using the *MatlabTM* function "ode45" which has been used to solve the differential equation of the RL circuit presented in chapter 2.

$$[t, i_c] = \text{ode45}(@\text{ElectricFunction}, tspan, x0);$$

Some fictitious parameters has been set up and a characteristic display of results is presented in figure 4.1.

```
*****Electric Circuit*****
Resistance:           1 [Ohm]
Voltage:              1 [V]
Final current:        0.99976 [A]
Inductance:            0.053296 [H]
Time constant:         53.2959 [ms]
Time for 99% saturation: 266.4793 [ms]
*****
```

Figure 4.1: RL Circuit Simulation Example

As we can see from the previous figure the results seems coherent with the theory, in fact once fixed the voltage and the resistance of the circuit, the value of the current at saturation diverge from the Ohm's laws by a negligible quantity. The time for 99% saturation has been computed as 5 times the time constant of the circuit.

From this code a graph has been derived and showed in the next figure.

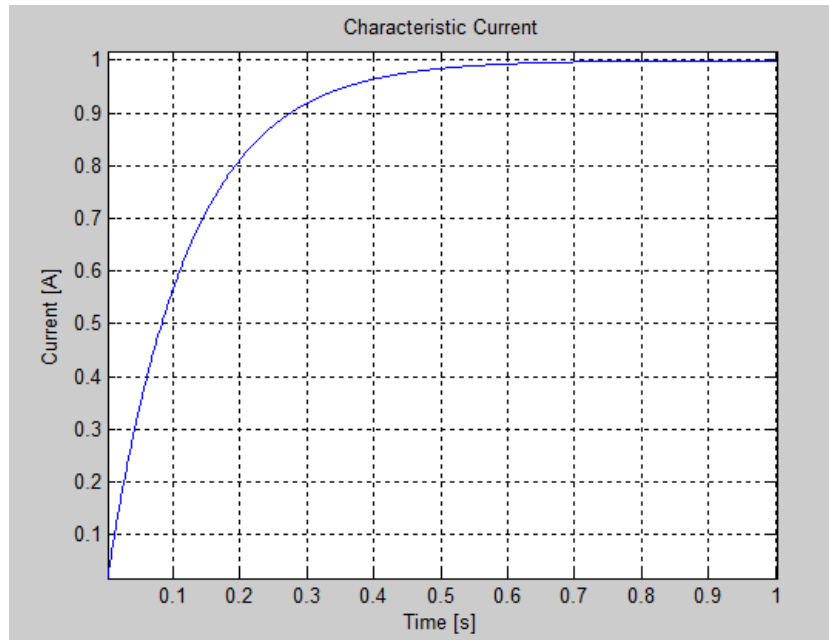


Figure 4.2: RL Circuit Simulation Graph

The characteristic current curve derived by the code has the classical shape of the ones founded in literature, so we can assume that the accuracy of the codes is enough to have a first order approximation of the real case. The *MatlabTM* code is reported in the appendix.

4.2.2 Spring Code

This code describe the behavior of a classical spring. The spring constant has been founded using the environment "Workbench" of the software *AnsysTM*.

```
.....Spring Force.....  
Material: Titanium Alloy  
Spring constant: 0.756 [N/mm]  
Preload spring lenght: 1.07 [mm]  
Maximum spring displacement: 1.29 [mm]  
Spring force with minmum air gap: 0.97524 [N]  
Spring force with maximum air gap: 0.80892 [N]  
.....
```

Figure 4.3: Spring Simulation Example

In this case the initial and the final position of the spring could be obtain by the drawings of Aerospazio Tecnologie s.r.l. Starting from this, using the list of materials contained in the catalog of the software *AnsysTM* has been founded the right material for the spring. At this point has been applied 1 N of force to the spring and the spring constant has been obtained by the classical formulation reported in chapter 2.

The graph of the variation of the force applied by the spring with respect to the displacement of the plunger is reported in the figure below.

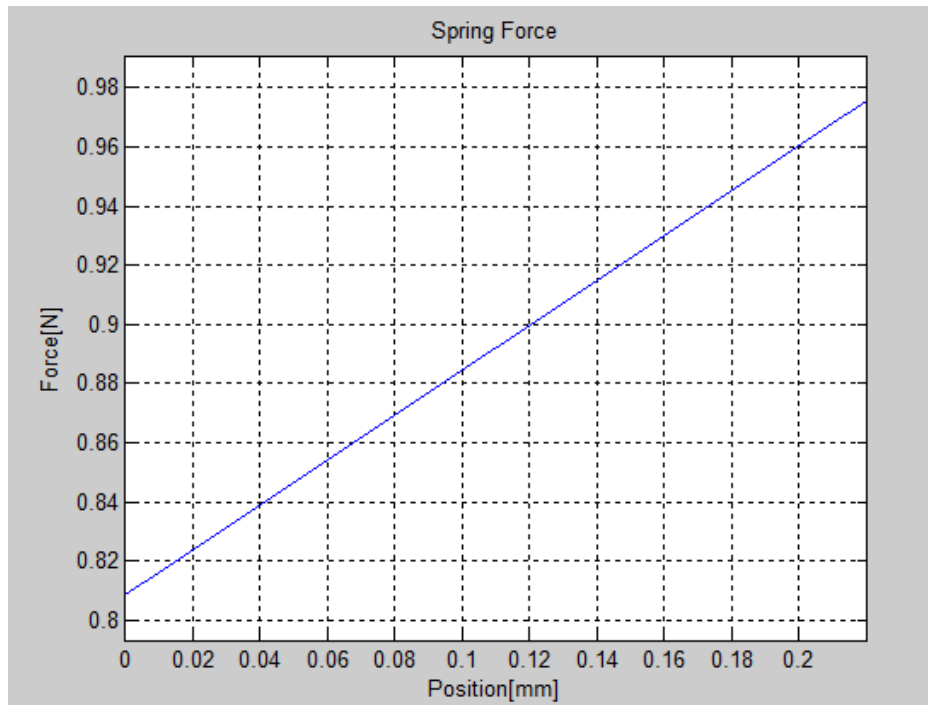


Figure 4.4: Spring Simulation Graph

The *MatlabTM* code is reported in the appendix.

4.2.3 Magnetic Code

This code has been created in order to describe the variation of the magnetic force with the displacement of the plunger. Moreover a differential study for the total circuit and the only air gap has been done. The result of the magnetic force simulation are reported in figure 4.5.

```
oooooooooooooo°Magnetic circuit°ooooooooooooo
Load current: 1 [A]
Number of turns: 300 []
Magnetic force with minimum air gap: 35 [N]
Magnetic force with maximum air gap: 14 [N]
Not approximated MF with minimum air gap: 34 [N]
Not approximated MF with maximum air gap: 14 [N]
oooooooooooooo.....
```

Figure 4.5: Magnetic Force Simulation Example

As we can note, there isn't a relevant differences between the approximated magnetic circuit and the complete one. The reasons of this behavior are multiple. Firstly the forces at work are of the order of the tens of Newton, so the difference cannot be properly appreciated. Secondly the relative permeability of the magnetic material is 4 order of magnitude greater than the vacuum one, this is multiplied for the length of the air gap which is just 2 order of magnitude smaller than the entire magnetic circuit, so this fact affect strongly the equation of the magnetic force and make the other terms of negligible in respect to the one related to the air gap.

The load current and the number of turns have been taken from literature.

From this code the graph of the variation of the magnetic force with the displacement of the plunger is reported in the figure below.

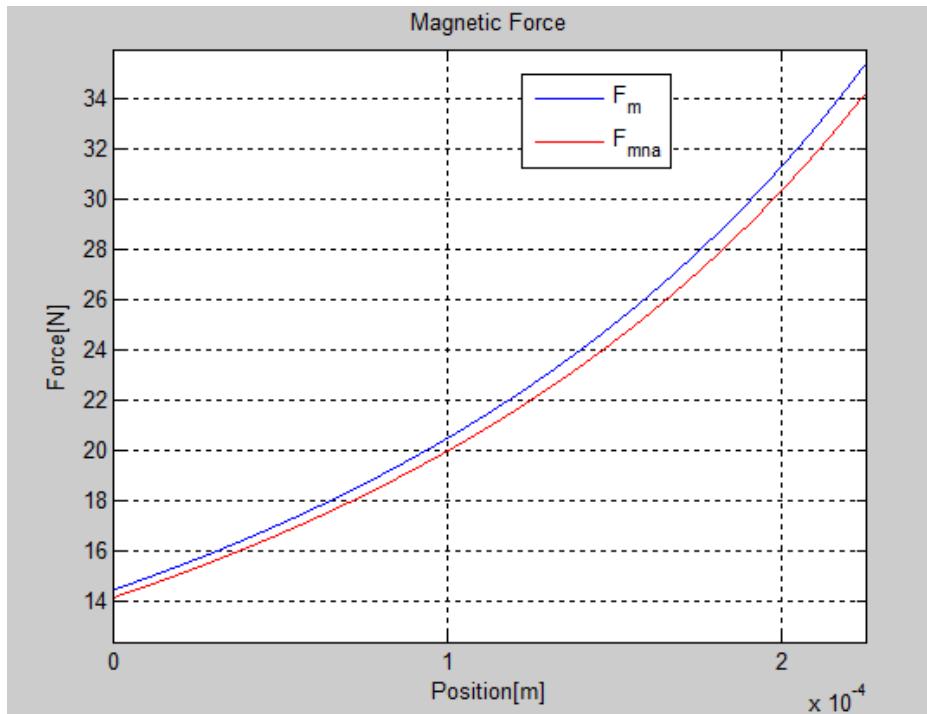


Figure 4.6: Magnetic Force Simulation Graph

This graph allows us to appreciate better the differences between the two models, the approximated force results in a overestimation of the true force exerted between the two magnets. Then, in order to be as much conservative as possible, in the main code has been implemented the not approximated magnetic force. The *MatlabTM* code is reported in the appendix.

4.2.4 Heating Code

This code has been created in order to describe the variation of the temperature as function of the time for different electric currents applied to the coil. The result of the heating up simulation are reported in figure 4.7.

```
.....Heating Results.....  

Diametro filo [mm]: 1  

Lenght of the wire [m]: 10  

Weight of the wire [g]: 70.3717  

1st Current [A]: 6  

1st Time to fusion [s]: 711.7639  

2nd Current [A]: 12  

2nd Time to fusion [s]: 177.941  

3rd Current [A]: 18  

3rd Time to fusion [s]: 79.0849  

.....
```

Figure 4.7: Heating Simulation Example

The length and the diameter of the wire has been taken from literature for this simulation. The first case represent the empirical recommended limit for a Copper wire of this diameter. The results obtained seems to be below the expectations, this is due to the conservative approach used to obtain our formula. We have to underline that the electric resistivity of the Copper derived by the equation 4.6 has been taken as constant at the temperature of fusion. This give us another conservative hypothesis which justify our results. From the second and the third cases we can appreciate the variation in the time to reach fusion of the same Copper wire for different electric current.

A better interpretation of the results can be seen using the following graph,that has been generated using the same code.

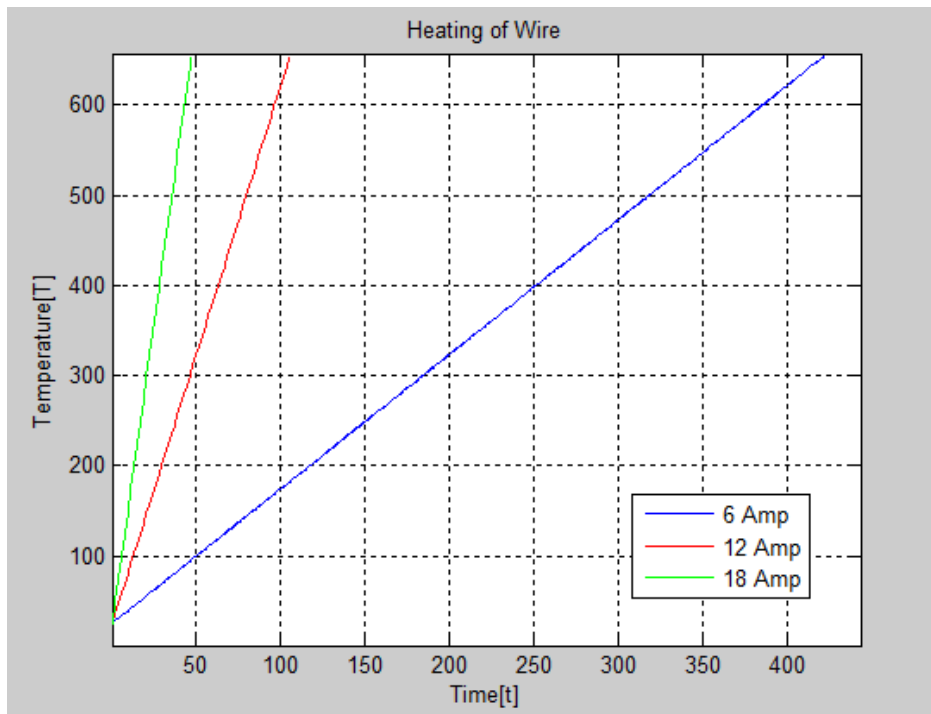


Figure 4.8: Heating Simulation Graph

This graph shows us how much the variation of the electric current changes the inclination of the characteristic curve temperature-time. The *MatlabTM* code is reported in the appendix.

4.3 Main Codes

In this section the results of the main codes used to set up the experiments has been reported. In both of these codes has been created a vector with multiple diameter of Copper wire in order to show how this parameter affect the characteristic of the valve.

4.3.1 Power Fixed Code

The first code has been developed keeping the power constant in order to identify the changes in the other parameters. This first approach has been followed because of the usual the power limitation requirement for the on-board system. This code can be utilize to see the changes in the magnetic and electric properties of the valve for a fixer power limit, so from literature the power limit of 5 Watt has been selected and the other parameters derived.

The result has been shown in the following figures.

```
*****Copper Coil Results*****
Power [W]: 5
Number of turns: 300
Inductance [H]: 0.78332
Diametro filo [mm]: 0.56 0.8 1.3
Length of the wire [m]: 9.16088 11.8752 17.5301
Weight of the wire [g]: 20.65812 54.38422 210.8606
Space Factor [%]: 0.281 0.57348 1.5143
Voltage [V]: 1.8115 1.4402 1.074
Resistance [Ohm]: 0.65633 0.41486 0.23068
Current [A]: 2.7601 3.4717 4.6557
Time to fusion [s]: 317.55315 835.98509 3241.3137
Time constant [ms]: 1193.4829 1808.1737 3395.7277
Time for 99% saturation [ms]: 5967.41451 9440.86826 16978.6385
*****
```

Figure 4.9: Power Fixed, Electric Simulation

This part of the code's display gives us information about the physical

characteristics of the coil, the electric current which flows through it, the time to "fusion" of the coil and the time response of the system. The time to "fusion" is computed in the adiabatic case with a large safety margin, so it must be intended as the time to reach the tolerable temperature by the coil.

```
*****Magnetic Circuit Results*****
Total Reluctance [1/H]:      5421545.4991
Traferro Reluctance [1/H]:    4981375.7936
Flux density through Air gap [T]:   1.5297      1.924      2.5802
Flux density through part 1 [T]:    12.964     16.3062     21.8675
Flux density through part 2 [T]:    0.81279     1.0223     1.371
Flux density through part 3 [T]:    33.0154     41.5269     55.6897
Magnetic Field through 0 [A/m]:    1217281.0492     1531100.5999     2053284.7835
Magnetic Field through 1 [A/m]:    687.76379     865.07184     1160.1059
Magnetic Field through 2 [A/m]:    43.12       54.2365     72.7339
Magnetic Field through 3 [A/m]:    1751.5207     2203.0692     2954.4293
Max Magnetic Force [N]:          268.8253     425.3004     764.8684
Min Magnetic Force [N]:          110.1108     174.2031     313.2901
*****
```

Figure 4.10: Power Fixed, Magnetic Simulation

The second part of the code's display gives us various information such as the reluctance of the magnetic circuit, the inductance of the air gap, the magnetic flux density and the magnetic field created in the magnetic circuit. In the end it shows us the changes in the force exerted between the magnets for the minimum and the maximum air gap. We must precise that the results presented in the previous figures will be calibrated using some corrective coefficients which have been obtained thanks to the experiments.

4.3.2 Ampere-Spire Fixed Code

The second code has been developed with the aim to understand how the various parameters change keeping the ampere-spire constant. This second approach has been followed once the minimum force to open the valve has been fixed, in our case by experiments. So after several attempt a minimum of 750 AS has been selected and the other parameters derived.

The results have been shown in the following figures.

Copper Coil Results			
Ampère-Spire [A]:	750		
Number of turns:	280		
Diametro filo [mm]:	0.56	0.8	1.3
Lenght of the wire [m]:	8.55016	11.0835	16.3614
Weight of the wire [g]:	19.31034	50.81866	196.9618
Space Factor [%]:	0.26227	0.53524	1.4134
Power [W]:	4.4018	2.7813	1.546
Voltage [V]:	1.6433	1.0384	0.57716
Resistance [Ohm]:	0.61351	0.38766	0.21547
Current [A]:	2.6786		
Current Density [A/mm ²]:	10.8752	5.32885	2.01803
Time to fusion [s]:	337.17612	1404.3154	9792.1512
Inductance [H]:	0.68236		
Time constant [ms]:	1112.22	1760.213	3166.7943
Time for 99% saturation [ms]:	5561.10004	8801.06485	15833.9713

Figure 4.11: Ampere-Spire Fixed, Electric Simulation

This first part of the code's display shows us several information for different wire diameter, and among these, power, current density, time to "fusion" and time response of the system. It has to be underlined that in order to fix the ampere-spire, also the number of turns has been taken as constant, this operation allowed us to keep variable the electric current.

```
.....Magnetic Circuit Result.....
Total Reluctance [1/H]: 5421545.4991
Traferro Reluctance [1/H]: 4981375.7936
Flux density through Air gap [T]: 1.3855
Flux density through part 1 [T]: 11.7424
Flux density through part 2 [T]: 0.7362
Flux density through part 3 [T]: 29.9043
Magnetic Field through 0 [A/m]: 1102573.2337
Magnetic Field through 1 [A/m]: 622.9539
Magnetic Field through 2 [A/m]: 39.0567
Magnetic Field through 3 [A/m]: 1586.47
Max Magnetic Force [N]: 220.5481
Min Magnetic Force [N]: 90.3365
.....
```

Figure 4.12: Ampere-Spire Fixed, Magnetic Simulation

The second part of the code's display exploit the strong dependence between the main magnetic characteristic of the valve and its ampere-spire. In fact once that the ampere-spire has been fixed, also all its magnetic properties has been appeared constant. This allows us to found the minimum force to open the valve and so the minimum ampere spire. Now becomes necessary to calibrate these results with the experimental ones.

4.4 Empirical Coefficient

In this section the modifications done on the codes after the experiments has been presented. This revision of the code has been used for a better calibration between the simulated model and the real one. In order to do this, a dimensionless and empirical coefficient has been introduced.

The first coefficient has been used to correct the divergences about the opening mechanism between the spring's code and the magnetic code. In fact, one strong assumption done regards the magnetic saturation of the magnetic circuit. It also affects the magnetic force exerted between the magnets, so the coefficient Ψ has been introduced in the code. It has been defined has:

$$\Psi = \frac{F_{spr_{max}}}{F_{mag_{min}}} \quad (4.1)$$

Where $F_{spr_{max}}$ represent the maximum force applied by the spring and $F_{mag_{min}}$ is the minimum force exerted by the magnets. The assumption on which is based this procedure is that the modeled and the real spring's force are the same. This can be done because of the relative simplicity of the spring's force determination. Once that this coefficient has been defined it has been introduced in the main code the empirical magnetic flux as:

$$\varphi_E = \Psi \cdot \varphi \quad (4.2)$$

After the integration of this parameter in the main code the saturation limit of every parts of the magnetic circuit has not been exceeded.

Chapter 5

Tests and Apparatus

In this chapter will be show the tests and the apparatus that has been used to tests the valve among Aerospazio Tecnologie s.r.l. First of all multiple instruments for vacuum's measurement will be presented and a common set up for a vacuum chamber will be described. Then will be presented the experiments made and the results obtained.

5.1 Vacuum Apparatus

In this section the classical instruments used in vacuum environment will be listed and explained, then the set up for vacuum chamber utilized during the experiments will be described and reported.

5.1.1 Vacuum Gauges

A vacuum gauges is an instrument used to measure the grade of vacuum, or pressure, in a certain environment. Firstly we must clarify that no one gauge can handle the entire range of vacuum pressures that we can produce, so we can use a combination of gauges or we can focus only in those range of pressure significant for our treatise. Secondly regardless of the care with which a gauge is manufactured and calibrated, the pressure read by the gauge may be different from the actual system pressure due to several reasons.

The placement of the gauge in the system is important. The pressure in the gauge will not usually be the same as the pressure in the vacuum chamber, because of the conductance of the connecting pipes. Some gauges act as sources of gas due to excessive outgassing while other gauges actually act as pumps. Usually for ultra-high vacuum measurements gauges are used that sit in the chamber without any tabulation.

The majority of the gauges react differently to different gases, so the knowledge of the gas composition is needed if we want to know the pressure exactly. As gauges are exposed to a variety of atmospheres in a system, their characteristics may change. Ideally the calibration of the gauges would be done periodically, but this is rarely done due to the expense and difficulty of this process.

We can divide gauges into different categories:

- Gauges that measure the pressure directly (force per unit area) or based on the force it applies. These include the liquid and capacitance manometers.
- Gauges that operate by measuring a quantity that is pressure sensitive such as thermal conductivity or viscosity.
- Gauges that ionize the gas and measure the amount of ionization which is proportional to the pressure. These include hot and cold cathode ionization gauges and the Residual Gas Analyzer. Note that these are the gauges we are interested in

A detailed descriptions of the working principles of these gauges has been reported in the appendix.

In the next figure is shown the ranges of pressure in which the different gauges operate.

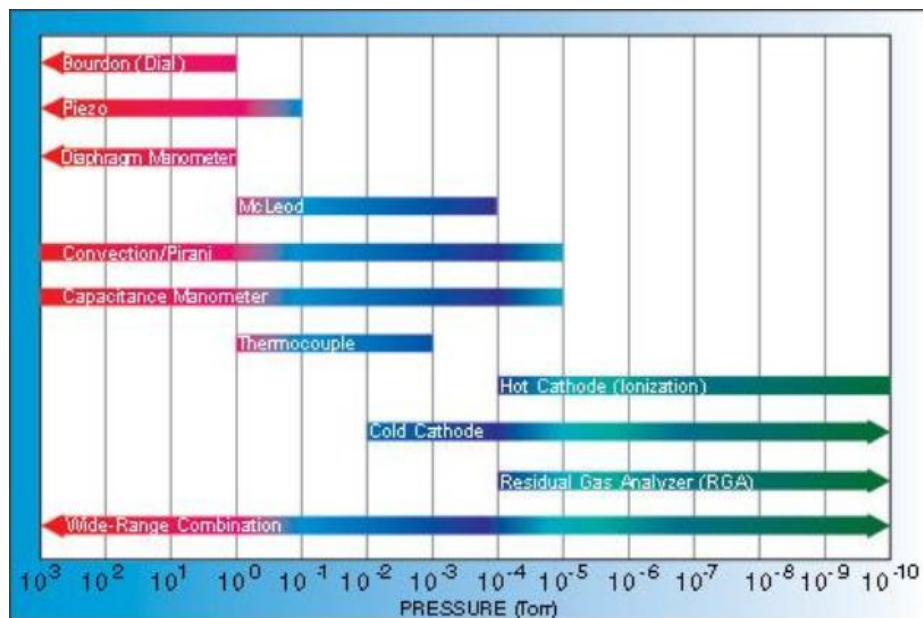


Figure 5.1: Operational Ranges of Vacuum Gauges

5.1.2 Leak Detector

A leak detector is an instrument used to identify and measure a leak of systems which contain liquids and gases. These instruments usually measure the leak rate of a system, it is the volume or the mass of fluid lost per second by the system for a fixed difference in pressure [$\text{bar} \cdot \frac{\text{m}^3}{\text{s}}$].

The requirements of a leak detector can be defined as:

- Sensitivity: Leak detectors have to sense a leak as small as possible.
- Reliability: Leak detectors have to guarantee to the user the lower numbers of detection errors.
- Accuracy: Leak detectors have to measure in detail a leak rate.

- Robustness: Leak detectors should continue to operate in non-ideal circumstances.

Leak detectors can be based on different leak detection techniques depending on the grade of precision they must ensure. The leak detector that has been used in our experiment is an electric one, which uses a foam-spray test.

5.1.3 Vacuum Chamber

A vacuum chamber is an instrument used to create a circumscribed vacuum environment. As vacuum gauges can't measure different grades of vacuum, so vacuum chambers need different types of pumps in order to reach the highest grades of vacuum, or the lowest pressure. Medium and large vacuum chambers have a cylindrical shape but usually the basis at the extremities of the cylinder are rounded, this makes them able to resist to lower pressures. Small chamber has various shapes depending on their application requirements.

The material of these chambers is usually a metallic one, anyway the choice of the material is quite crucial and depends from several factors such as strength, pressure, and permeability.

A list of the common material used is now reported.

- Stainless Steel
- Aluminum
- High density ceramic
- Glass

Vacuum chambers have usually multiple portholes in order to allow the installation of instruments or windows in the walls of the chamber. In low

to medium vacuum applications these portholes are sealed with common o-rings, whereas in higher vacuum applications the junction is a copper gasket bolted between the two pieces.



Figure 5.2: Medium Vacuum Chamber

A type of vacuum chamber frequently used in the field of spacecraft engineering is a thermal vacuum chamber, which provides a thermal environment representing what a spacecraft would experience in space.

5.2 Experiments Set Up & Results

In this section the experiments set up has been presented following the chronological order in which they has been conducted. Then the results for any experiments has been reported and discussed.

5.2.1 Leak Rate Evaluation

The first experiment regard the evaluation of the leak rate of the valve for an assigned difference in pressure. As said the previous chapter the tightness of the valve depend principally from two factor: the pre-load force of the spring and the type of material of the part beated by the plunger, in addiction to the shape of the beating surface. For the first factor, the pre-load spring force, can be said that the leak rate of the valve decrease with the growth of the pre-load force, probably in a non linear way. For the second factor has been tested that the original seat material, the Vespel SP1, granted an insufficient tightness capacity of the valve. So the original piece has been substituted with a part in Silicone.

The instruments used in this experiment were:

- Leak detector
- Pipeline
- Helium tank

The valve has been connected to the leak detector by an apposite pipeline. This connector had the function to allow or deny the passage of gas between the valve and the leak detector. At this point the valve has been putted at rest and consequently it has been closed. The pipeline has been opened and so the passage of gas between the valve and the leak detector has been guaranteed. In this situation both the valve and the leak detector had an internal pressure equal to the environmental pressure, which is approximately 1 bar.

The set up of these experiment has been schematized in the next figure.

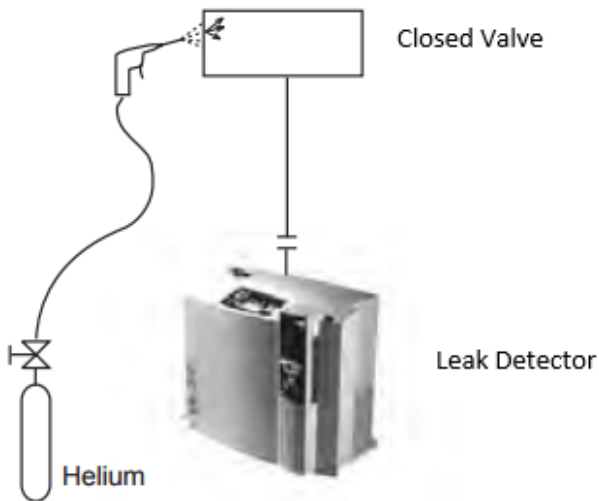


Figure 5.3: First Experiment Scheme

At this point the leak detector has been activated and it has been set at different pressures in order to create different levels of vacuum. When the pressure in the valve has been stabilized and the equilibrium condition has been reached, some Helium particles have been sprayed against the nozzle of the valve. Doing this major quantity of particles has been stopped by the closure mechanism of the valve whereas a smaller quantity of particles has been able to pass through the gasket of the valve and they have been registered by the leak detector.

In the following figure can be seen the leak detector and the valve used for this experiment, moreover in the display of the leak detector can be appreciated the result of the experiment.



Figure 5.4: Leak Rate Experiment

This experiment has been done for two different value of pressure with great results in both cases. The case with the Vespel SP1 gasket has been added to the table from data of a previous experiment conducted by Aerospazio Tecnologie s.r.l. because of the impossibility to test the first version of the gasket. A small table with the data is now reported.

	Gasket Material	Pressure Set [bar]	Leak Rate [mbar · $\frac{l}{s}$]
Test 1	Vespel SP1	$4,3 \cdot 10^{-3}$	Saturation
Test 2	Silicone	$4,3 \cdot 10^{-3}$	$1,8 \cdot 10^{-8}$
Test 3	Silicone	$5,1 \cdot 10^{-4}$	$6,7 \cdot 10^{-8}$

Table 5.1: Leak Rate Results

These tests have been done in the range of $10^{-3} - 10^{-3}$ bar because this

is the nominal operating pressure for a common XFS. The obtained results are several order of magnitude better than the nominal leak rate of the valve available on the market. The reason of this difference should be attached to the choice of the gasket material. In fact the Silicone is particularly adapt to avoid the leakage of the particles from the valve. However this material has not been used in space because of its decreasing in performances due to the variation of temperature. Moreover it high malleability could created problems of deformation related to the tiny characteristic dimensions of these applications. Any way the great impact of the Silicone in stopping the particles leakage has been demonstrated, other tests should be done in future to verify in which range of temperatures its performance remains better than the other gasket materials.

5.2.2 Minimum Force Identification

This second experiment concern the individuation of the minimum value of ampere-spire which generated enough magnetic force to open our valve. Obviously the ampere-spire value is related both to the current which flows through the coil and to the number of turns.

The instruments used in this experiment were:

- Tester
- Power supply
- Connectors

This experiment has been done for the two best simulated configurations derived from the codes described in the previous chapter. The coils tested have been composed by two wire of respectively diameter of 0,56 mm and 0,8 mm.

In the following figures the two new configuration of the coils has been reported:

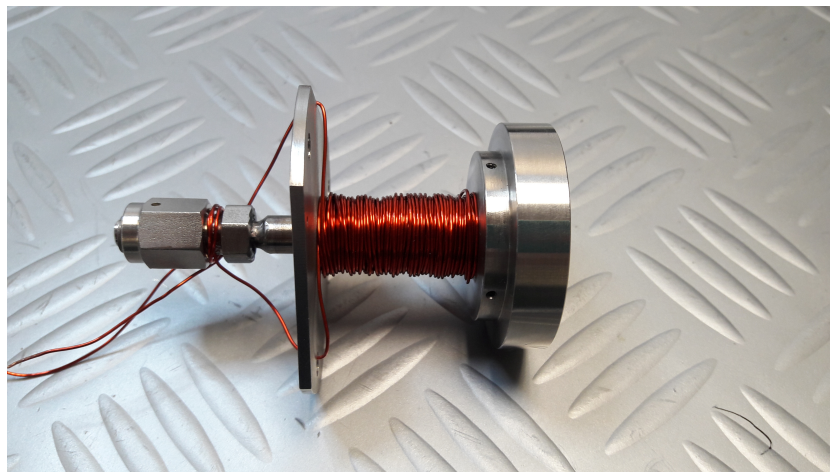


Figure 5.5: First Coil Configuration 0,56 mm

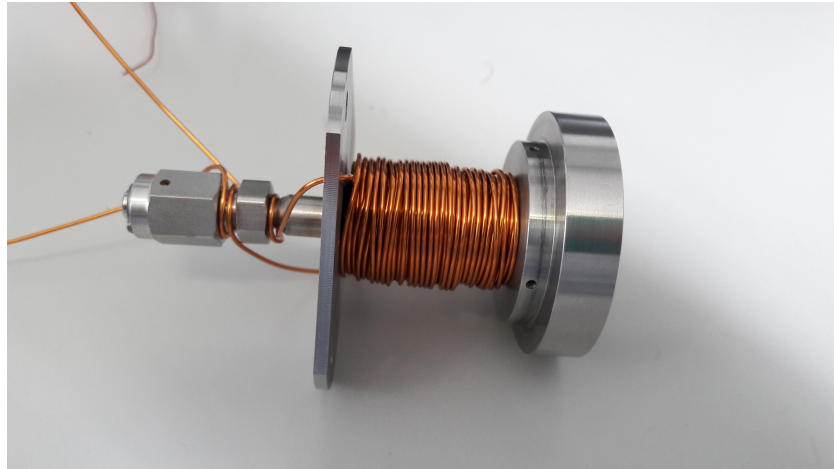


Figure 5.6: Second Coil Configuration 0,8 mm

Moreover the first version of the coil has been tested to have a method of comparison between the various configuration, it must underlined that the diameter of the wire used was 1,3 mm and this configuration has been found ready among Aerospazio Tecnologie s.r.l. On the contrary the two new configurations has been manually mounted and tested before the experiments.

When the coils has been prepared using an electric tester has been verified the perfect functionality of the coil. In fact a different of voltage between the two extremities has been applied and the resistance has been measured and compared with the simulated value. For the first configuration the resistance simulated was 0,77 Ohm whereas the resistance measured has a value of 0,81 Ohm. So the codes has been resulted quite accurate for this first test.

Once that the functionality of the coil has been ensured the coil has been attached to the power supply by two apposite connectors. The power supply used is Tdk-lambda zup 36-6 and has the capability to give an electric current in the range from 0,5 A to 5 A.

A picture of the set up of the experiment has been reported:

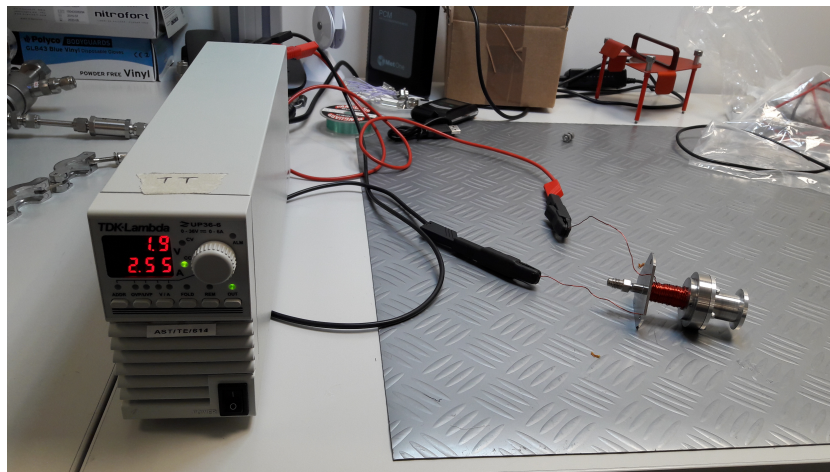


Figure 5.7: Second Experiment Set Up

It has to be underlined that the same assembly of the valve which concern the mechanism of opening and closure has been used for the different configurations. In other words, the only part that has been changed between one and the other configurations was the coil of the valve.

The data required from this experiment has been collected in the following table:

Wire Diameter [mm]	Voltage [V]	Number of Spires []	Ampere for Opening [A]
0,56	2	252	2,55
0,8	1,4	280	2,3

Table 5.2: Minimum Amperage for Opening

The first configuration that has been tested had a coil of 0,56 mm wire diameter and 252 number of turns. After several trials has been founded that the minimum amperage which allows the opening of the valve was 2,55 A.

The second configuration tested had a coil of 0,8 mm wire diameter and 252 number of turns. It has been identified 2,33 as minimum amperage.

As can be seen from equation 2.12 the magnetic force is proportional to the ampere-spire of the coil, from these experiments has been obtained that the minimum ampere-spire that we have to guarantee in order to open this valve is 644 AS. Starting from these results the corrective coefficients showed in section 4.4 has been introduced in the model. Moreover this experiment has confirmed the effectiveness of the simulations.

5.2.3 Temperature Rising Experiment

This third and final experiment regard the evaluation of the variation of temperature of the coil for different period of operation both in air and in vacuum environment. In the first part of this experiment the variation of temperature of the coil has been tested in air.

The instruments used in this part were:

- Thermocouple
- Temperature calibrator
- Kapton tape
- Chronometer
- Power supply
- Connectors

The set up of the electric part has been utilized again the same of the previous experiment, however a thermocouple has been fixed, using a kapton tape, to the external part of the coil. The other extremity of the thermocouple has been connected to a temperature calibrator which had the aim of displaying the temperature of the coil. The model of the temperature calibrator was FLUKE 724.

The figure of the set up of this first part of the experiment has been reported:



Figure 5.8: Temperature Experiment Air Set Up

From the previous figure can be seen the first configuration tested. This experiment has been repeated at three different current for the two different configuration of 0,56 mm and 0,8 mm wire diameter. In order to have some data compatible with the valve functionally, the minimum amperage for both configuration has been tested. Moreover an extra value of current has been given in order to see more appreciable differences for the same configuration.

The procedure used is simple, when all the components have been connected each other, the initial temperature has been recorded. At this point both the power supply and the chronometer have been activated at the same time and the value of temperature has been transcribed for every time interval.

The data required from this experiment has been collected in the following tables:

Current [A]	Time [s]				
	0	30	60	120	180
1,15					
0,56 mm Temperature [°C]	22,6	24,8	26,5	29,4	31,4
0,8 mm Temperature [°C]	21,6	22,5	23,1	24,2	25,1

Table 5.3: Temperature Rising Results in Air for 1,15 A

Current [A]	Time [s]				
	0	30	60	120	180
2,3					
0,56 mm Temperature [°C]	23,8	31,6	39,2	50,9	58,7
0,8 mm Temperature [°C]	22,9	25	27,4	31,4	34,8

Table 5.4: Temperature Rising Results in Air for 2,3 A

Current [A]	Time [s]				
	0	30	60	120	180
2,55					
0,56 mm Temperature [°C]	25,8	36	45,1	58,9	69,1
0,8 mm Temperature [°C]	26,4	28,8	31,4	35,8	39,2

Table 5.5: Temperature Rising Results in Air for 2,55 A

From the previous tables it is possible appreciate the different rise in temperature for the two configuration. As expected, the coil with the wire diameter of 0,8 mm shows a lower increase in temperature for any current applied. It must be precised that it has not been possible start every prove from the same initial temperature for practical reasons.

Using again the software *MatlabTM* the data collected has been interpolated in order to verify the simulated model. The results of the interpolation

has been showed in the next figures:

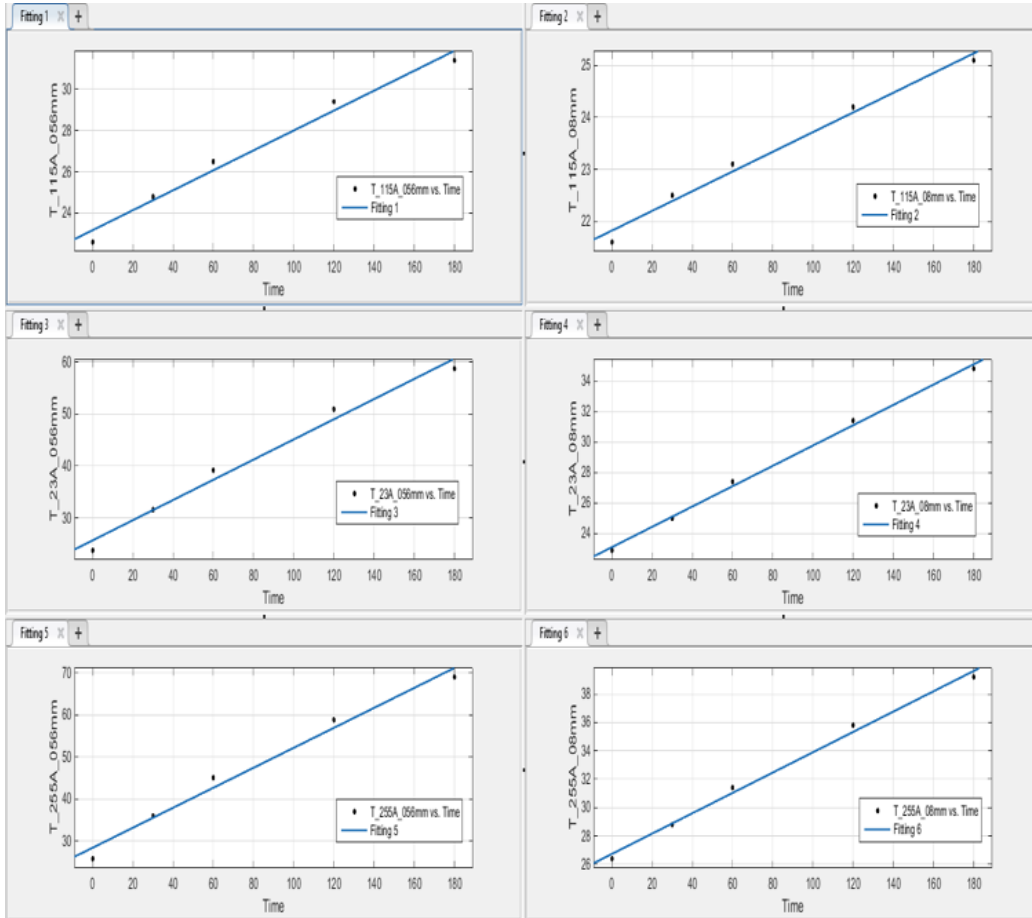


Figure 5.9: Temperature Fitting in Air

As we can see the data matched quite well with the fitting straight line which is in agreement with the simulated model. At least we can deduce that the simulated model is valid in this ranges of temperature and time.

In the second part of this experiment the previous procedure has been repeated in a small vacuum chamber. The instruments used in this part were the same utilized before, moreover a few more must be added:

- Oil pump
- Vacuum chamber
- Pressure scope
- Pressure display

The set up is also similar to the previous one, but this time the valve has been put in a vacuum chamber. The others instruments have been connected to the valve by apposite flanges and the low pressure has been created using an oil pump. During the experiment, the pressure has been stabilized around $2 \cdot 10^{-4}$ bar.

A photo of the set up is now reported:

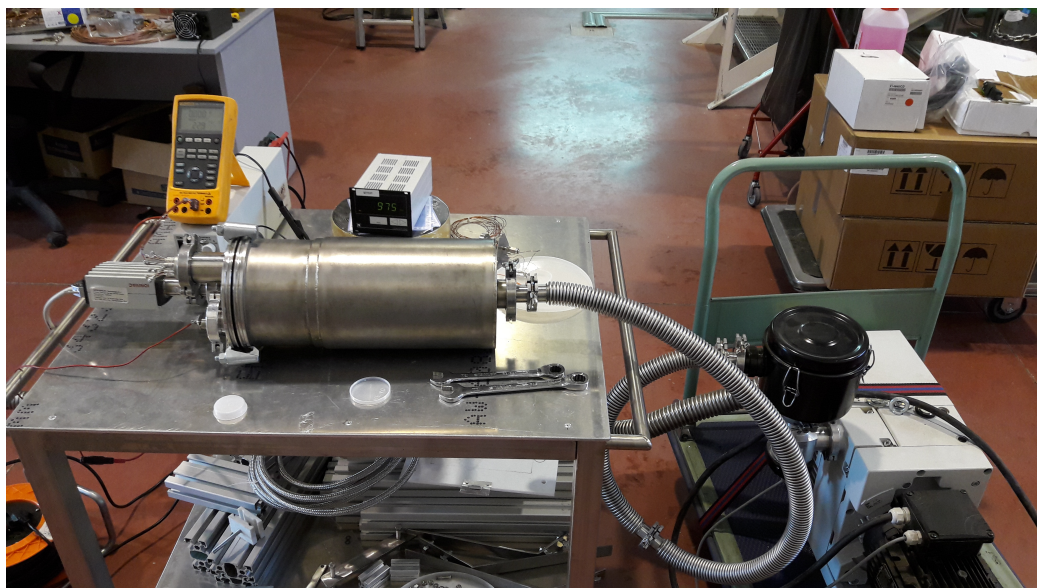


Figure 5.10: Temperature Experiment Vacuum Set Up

During this phase, the experiment has been repeated only for the minimum current which allows the opening of the valve. So for the first configuration the coil has been supplied with a current of 2,55 A, whereas for the second one with a current of 2,3 A.

	Time [s]					
	0	30	60	120	180	360
0,56 mm Temperature [°C]	22,1	28,6	37,2	53,4	67,6	∅
0,8 mm Temperature [°C]	22,9	23,7	25,4	28,9	32	40

Table 5.6: Temperature Rising Results in Vacuum

The interpolation of data is now reported.

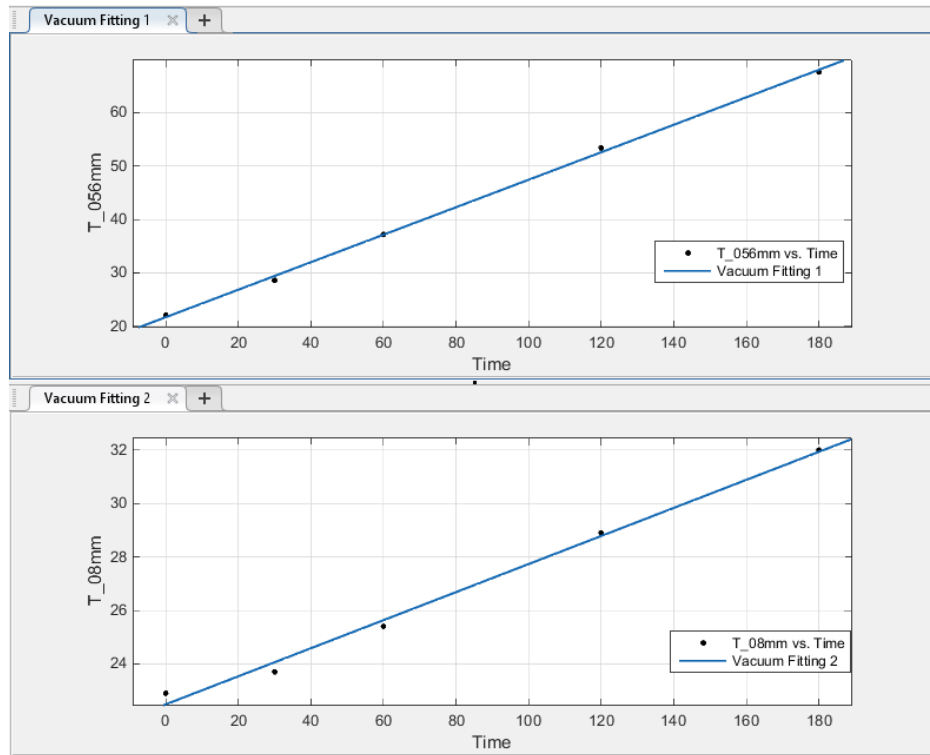


Figure 5.11: Temperature Fitting in Vacuum

The results of these experiments appear congruent with the previous line

of reasoning. However, if they are compared with the results of the same configuration in air they appear anomalous. This observation can be better valued with the help of following table:

Time [s]	Temperature [$^{\circ}\text{C}$]					
	0,56 mm 2,55 A			0,8 mm 2,3 A		
	Air	Vacuum	Difference	Air	Vacuum	Difference
0	25,8	22,1	-3,7	22,9	22,9	0
30	36	28,6	-5,4	25	23,7	-1,3
60	45,1	37,2	-7,9	27,4	25,4	-2
120	58,9	53,4	-4,5	31,4	28,9	-2,5
180	69,1	67,6	-1,5	34,8	32	-2,8

Table 5.7: Temperature Rising Comparison

As it can be seen from table 5.7, the comparison between the same coil configuration in air and in vacuum shows a greater increment of temperature in air rather than in vacuum. This behavior has gone against the one expected. In fact, it has been thought that in absence of convection, the dissipation of temperature would have been minor.

The explanation to this phenomena has been identified in the positioning of the thermocouple. The contact between the extremity of the thermocouple and the coil take place in the outer surface of the coil. Moreover a Kapton tape has been used to fix the contact created between the two pieces.

The positioning of these two elements has been schematized in the following figure.

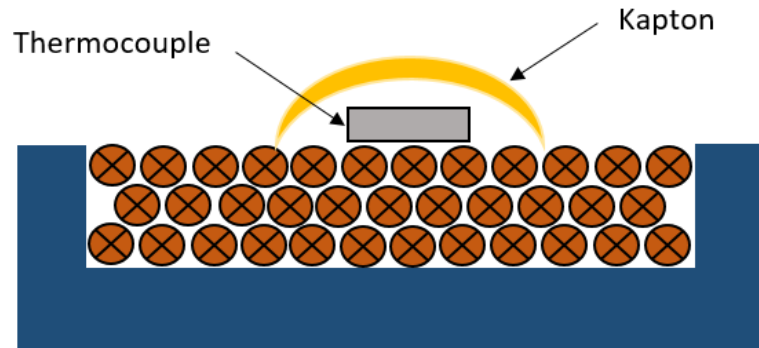


Figure 5.12: Scheme of Thermocouple Positioning

When the coil has been activated in air its temperature has started to rise up. However the increase of temperature is not homogeneous in the radial direction of the coil, the inner part tends to heat up faster than the outer part. The heat generated at the center can be transferred to the region of the thermocouple by conduction or by air convection. The conduction is not influential in this analysis because it is also present in vacuum. So the answer has been searched in the convective phenomena. The peculiar position of the kapton tape tends to trap the hot air which comes from the inner region of the coil. Furthermore the coil has been wrapped manually, this led the hot air to have an easily path between the turns of the copper wire. All these elements contribute in a substantial way to enhance the temperature measured by the thermocouple in presence of air.

In order to verify our assumption, the same experiment has been repeated measuring the voltage needed by the power supply to maintain the current constant. It has been found that even if the temperature measured in vacuum and in air was the same, the voltage needed in the vacuum configuration was higher than the one needed in air. So the effective resistance has been computed using the first Ohm's law. Then using the equations 2.34 and 2.35

the average temperature of the coil has been obtained. A scheme of these results is now reported.

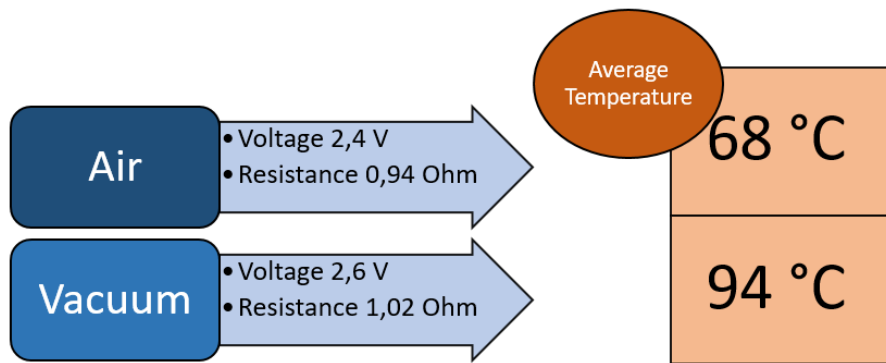


Figure 5.13: Average Temperature in Air and in Vacuum

From this it has been possible deduce that the medium temperature of the coil in vacuum was higher than the medium temperature in air, and so the increasing in temperature.

Conclusions

In this thesis, a nonlinear model for a electromagnetic gas exchange valve actuation system has been proposed. Due to the many constraints and requirements, the redesign and implementation of this valve has proven to be exceptionally challenging. The multi-disciplinary nature of the problem has also hindered development as the design involves insights of electricity, magnetism, heat transfer and control system theory.

The valve's configuration itself has been successfully modified. Due to the many variables and the high complexity of this mechanism, the largest number of modifications has regarded the external casing of the valve. A more compact and lighter closure mechanism has been proposed. However the design assumptions made, together with the data collected, have been demonstrated coherent with the subsequent study, thus this configuration has been proved to be a viable solution for a real Xenon Feeding System.

A *MatlabTM* code, representing the valve's main aspects, has been developed by the union and modification of smaller codes. It has turned out to be accurate for most of the valve's parameters, however part of the results has been derived because of the overcoming of the magnetic saturation limit, so a corrective and empirical coefficient has been introduced. Then the model derived has been calibrated by experimental verification and so its reliability has been verified.

The experiments done among Aerospazio Tecnologie s.r.l. have showed the optimal performances of the valve. Its tightness has been ensured by the utilization of a silicon gasket with excellent results, however further studies should be done on its long term functionality. The minimum magneto-motive force which allows the valve's opening has been individuated and verified for different wire diameters. The thermal capability of the different configurations has been tested both in air and in vacuum, thus data has been collected and the model confirmed. Further studies should be investigate the long term effects of the temperature.

Appendix A

High Vacuum Gauges

Every modern high vacuum and ultrahigh vacuum system relies on some form of ionization gauge for pressure measurements under 10^{-3} Torr. There are currently three types of ionization gauge technologies which allow us pressure measurements between 10^{-2} and 10^{-10} Torr:

1. The Hot Cathode Gauge (HCG) in which the ionizing electrons from a thermionic cathode are accelerated by suitable electrodes into an ionizing space.
2. The Cold Cathode Gauge (CCG) in which the ionization is caused by a circulating electron plasma trapped in crossed electric and magnetic fields.
3. The Residual Gas Analyzer (RGA) in which a scan of relative amplitude of different ionized species versus mass of the species is produced.

Note that the pressure is proportional to the number of molecules in the system. If we can count the molecules we can compute the pressure. If ionization of the molecules occurs, the positive ions can be collected and their current measured. The ion current is proportional to the number of ions in the chamber which is proportional to the number of molecules and hence the pressure.

A.1 Hot Cathode Gauge (HCG)

The basic types of Hot Cathode Gauges are two. The Bayard-Alpert gauge is capable to measure pressures from 10^{-3} to 10^{-11} Torr, instead the Schultz-Phelps gauge can measure higher pressure as 1 Torr, but cannot measure pressure under 10^{-6} Torr. The Bayard-Alpert gauge (BAG) heat up electrons by a hot filament and accelerate them toward a cylindrical grid cage. As the electrons traverse the space enclosed by the grid, which is fully open to the vacuum chamber, they collide with gas molecules ionizing some of them. A fine wire located at the center of the ionization volume collects the resulting cations producing a current proportional to the gas density at the gauge.

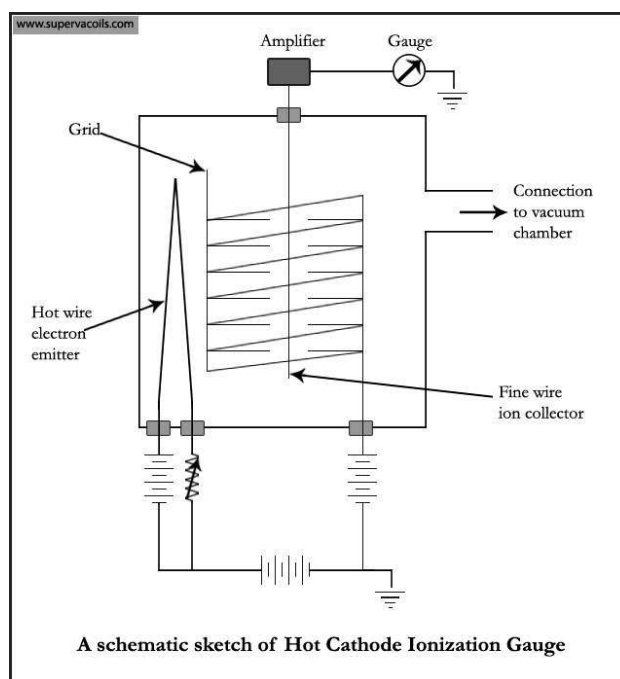


Figure A.1: Hot Cathode Gauge Scheme

At constant temperature, the collector current is linearly related to the gas pressure. The linear dependence of collector current on pressure is the most important advantages of these gauges. The deviations from linearity

typically amount to less than $\pm 25\%$. In respect of the true value of pressure, obviously the biggest deviations take place at the operating limits.

The collector current i_c is proportional to the ionizing current (filament current) i_e and the reading pressure p_r is proportional to the collector current. We can put these together to get:

$$p_r = \frac{i_c}{S \cdot i_e} \quad (\text{A.1})$$

Where S is the gauge sensitivity. For the Bayard-Alpert tube the sensitivity is about 9.3^{-1} Torr, so if the filament current is 20 mA and the collector current is 0,03 mA, the pressure is $1,6 \cdot 10^{-4}$ Torr.

The gauge is very sensitive to the composition of the gas because of their ionization energy which changes between gas species. Gauges are generally calibrated for Air or Nitrogen, so the true pressure is given by the pressure reading multiply by the gas correction factor. It is computed experimentally, some data is reported in the following figure:

For a chamber containing Xenon and showing a pressure of $1,6 \cdot 10^{-4}$ Torr, as in the previous example, the true pressure can be computed from the reading pressure multiply by the gas correction factor, which is 0,34 for Xenon. It can be expressed in a simple formula as:

$$p_t = C \cdot p_r \quad (\text{A.2})$$

Where C is the gas correction factor and p_t is the true pressure. In our case can be easily obtained a true pressure of $5,44 \cdot 10^{-5}$ Torr.

Gas Type	Gas Correction Factor
Air/Nitrogen	1.00
Acetone	0.28
Argon	0.77
Carbon Dioxide	0.71
Carbon Monoxide	0.95
Chlorine	1.47
Deuterium	2.86
Ethanol	0.28
Ethylene	0.43
Helium	5.56
Hydrogen	2.17
Krypton	0.53
Methane	0.71
Methanol	0.56
Neon	0.3
Nitrous Oxide	0.67
Oxygen	1.00
Water	0.91
Xenon	0.34

Figure A.2: Gas Correction Factor

A.2 Cold Cathode Gauge (CCG)

This type of gauge is also called Penning Gauge. The electrons are emitted from a cold cathode (room temperature) when we apply a large enough voltage, typically the high voltage ranges from 2-6 kV. If we accelerate the electrons with the same field as was used to extract them, we can have energetic electrons capable of ionizing the gas in the system. We can trap the electrons and increase their mean free path by applying a magnetic field, usually it is and the magnetic field 0,1-0,2 T. The probability of collision between electrons and gas molecules is proportional to the gas density. The slow ions generated, are quickly captured by the cathode. The current generated by this ion collection process is measured and used as an indirect indication of gas density and pressure.

The current induced by ions is not linearly related to the pressure in the

chamber. Rather, the relationship is exponential and complicated by the presence of spurious discontinuities in the current vs. pressure characteristic curve. The number and size of discontinuities depends on gauge design, with the inverted magnetron being the least susceptible to this problem.

This gauge is sensitive to the composition of the gas in the same way as the Hot Cathode Gauge.

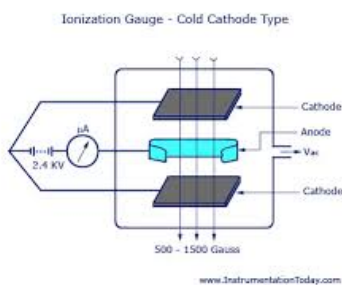


Figure A.3: Cold Cathode Gauge Scheme

A.3 Residual Gas Analyzer (RGA)

The Residual Gas Analyzer is a low-resolution mass spectrometer. It samples the gas in a system and typically produces a scan of relative amplitude of different ionized species versus mass of the species over a range of 1 to 200 amu (atomic mass unit). The Residual Gas Analyzer is used in most cases to monitor the quality of the vacuum and to determine the absolute partial pressures of gases in the system, but is more commonly used to indicate what species are present in the system. The pressure can be measured down to 10^{-14} Torr, even if the most commercially available systems reach 10^{-11} Torr.

It is a powerful analytical tool, in fact it can be used quantitatively to determine absolute partial pressures of the various gases in the system. Anyway its costs is prohibitive and should be used only in specific applications.

Appendix B

Matlab codes

B.1 Electric Circuit Code

B.1.1 Electric Function

```
%%Function
function i_dot = electricequation(t,i_c)
R = 1;                                %circuit resistance [0mh]
V = 1;                                %circuit voltage [V]
mu0 = pi*4e-7;                         %vacuum permeability[H/m]
N = 75;                               %number of turns []
k_m = 15000;                           %relative consant of vacflux []
muV = mu0*k_m;                        %vacoflux permeability [H/m]
r_core = .003;                          %raggio medio ferrocore [m]
S_core = pi*(r_core)^2;                 %sezione ferrocore [m^2]
l_sol = .025;                           %lunghezza solenoide [m]
L= (muV*S_core*(N)^2)/l_sol;          %inductance [H]
tau=(L/R)*1000;                        %circuit time constant [ms]
tau_r= 5*tau;                          %circuit time response [ms]
i_dot = [-i_c*(R/L) + V/L ]
```

B.1.2 Electric Editor

```

%% Solutore

tspan = [0:.001:1];
x0=[0, 0];
[t,i_c]= ode45(@ElectricFunction, tspan, x0);

%% Parameters

R = 1;                                %circuit resistance [0m]
V = 1;                                %circuit voltage [V]
mu0 = pi*4e-7;                         %vacuum permeability[H/m]
N = 50;                               %number of turns []
k_m = 15000;                           %relative constant of vacflux []
muV = mu0*k_m;                         %vacoflux permeability [H/m]
r_core = .003;                          %raggio medio ferrocore [m]
S_core = pi*(r_core)^2;                 %sezione ferrocore [m^2]
l_sol = .025;                           %lunghezza solenoide [m]
L= (mu0*k_m*S_core*(N)^2)/l_sol;      %inductance [H]
tau=(L/R)*1000;                         %circuit time constant [ms]
tau_r= 5*tau;                           %circuit time response [ms]

%% Graph

plot(t,i_c(:,1)), title('Characteristic Current')
xlabel('Time [s]');
ylabel('Current [A]');
grid on;

```

```
%% Display of Results

disp(' ')
disp('Electric Circuit')
disp(' ')
disp(['Resistance: ', num2str(R), '[Ohm]'])
disp(' ')
disp(['Voltage: ', num2str(V), '[V]'])
disp(' ')
disp(['Final current: ', num2str(i_c(1001)), '[A]'])
disp(' ')
disp(['Inductance: ', num2str(L), '[H]'])
disp(' ')
disp(['Time constant: ', num2str(tau), '[ms]'])
disp(' ')
disp(['Time for 99% saturation: ', num2str(tau_r), '[ms]'])
disp(' ')
```

B.2 Spring Force

```

%% Inizialization of variables

syms x
k = .756; %Spring constant [N/mm] = 756 [N/m]
l_0 = 1.07; %Preload spring displacement [mm]
l_final = 1.29; %Final spring displacement [mm]
F_s = k*(l_0+x); %Spring Equation
F_smax = k*(l_0); %Spring Maximum Force
F_smin = k*(l_final); %Spring Minimum Froce

%% Graph

ezplot(F_s, [0, .22])
grid on;
xlabel('Position[mm]');
ylabel('Force[N]');
title('Spring Force');

%% Display of Results

disp(' ')
disp('Spring Force')
disp(' ')
disp(['Material: ', 'Titanium Alloy'])
disp(' ')
disp(['Spring constant: ', num2str(k), '[N/mm]'])
disp(' ')
disp(['Preload spring lenght: ', num2str(l_0), '[mm]'])
disp(' ')

```


B.3 Magnetic Force

```
%% Inizialization of variables
```

```

syms x F_m;
mu0 = pi*4e-7; %vacuum permeability[H/m]
N = 300; %number of turns []
k_m = 15000; %relative consant of vacflux []
muV = mu0*k_m; %vacoflux permeability [H/m]
A_0 = (((pi*(.0155^2 - .001^2))/4) + ((pi*(.004^2 - .001^2))/4))/2; %sezione trafe
i0 = 1; %load current [A]
delta = .625e-3; %maximum stroke [m]
l_sol= .017; %lenght of solenoid
l_c = .1; %lenght of magnetic circuit[m]
```

```
%% Magnetic Equations
```

```

F_m = (mu0*A_0*(N*i0)^2)/(2*(delta - x)^2); %Approximated Magnetic Force
F_m_na = (mu0*A_0*(k_m*N*i0)^2)/(2*((k_m*(delta - x))+l_c)^2); %Not approximated M
F_mmax = (mu0*A_0*(N*i0)^2)/(2*(delta)^2); %Max Air Gap Magnetic Force
F_mmin = (mu0*A_0*(N*i0)^2)/(2*(.4e-3)^2); %Max Air Gap Magnetic Force
F_mmax_na = (mu0*A_0*(k_m*N*i0)^2)/(2*((k_m*delta) + l_c)^2); %Max Air Gap NA Magn
F_mmin_na = (mu0*A_0*(k_m*N*i0)^2)/(2*((k_m*(.4e-3))+l_c)^2); %Min Air Gap NA Magn
```

```
%% Graph
```

```

h1=ezplot(F_m,[0,.225e-3]);
hold on;
h2=ezplot(F_m_na,[0,.225e-3]);
set(h2,'color','r','linestyle','--')
```


B.4 Heating Effect

```

%% Initialization of Variables

l_wextra = 10; %lunghezza filo[m]
D_w=1e-3; %diametro filo[m]
S_w = (pi*D_w^2)/4; %sezione filo [m^2]
Cu_dens = 8960; %Copper density [kg/m^3
W_w = Cu_dens*l_wextra.*S_w; %Totale weight of the Copper wire
T = 25; %Tiniziale[°C]
T_fus = 1086; %T accettabile rame (T fusione 1086°C)
DT = T_fus - T; %Delta T accettabile
rho2 = 0.0156*(1 + 0.00428*T_fus)*1e-6; %Cu resistivity [Ohm*(m)]
i0=6; %saturation current [A]
i2=12; %saturation current [A]
i3=18; %saturation current [A]
R2 = (rho2*l_wextra)/S_w; %Coil Resistance [Ohm]
CS = 385; %Calore specifico Rame [J/(kg*°C)]]

%% Heating Equations

t_fus = (CS*W_w*DT)/(R2*(i0^2));
t_fus2 = (CS*W_w*DT)/(R2*(i2^2));
t_fus3 = (CS*W_w*DT)/(R2*(i3^2));

%% Graph

syms x
T_g = T+(R2*(i0^2)*x)/(CS*W_w);
T_g2=T+(R2*(i2^2)*x)/(CS*W_w);
T_g3=T+(R2*(i3^2)*x)/(CS*W_w);

```


B.5 Final Code

```

%% Inizialization of variables%%
T = 25; %temperature Celsius
rho = 0.0156*(1 + 0.00428*T)*1e-6; %Cu resistivity[Ohm*(m)]
Cu_dens = 8960; %Copper density [kg/m^3]

%Solenoide
r_c_ext = 15e-3; %raggio esterno solenoide [m]
r_c_int = 3e-3; %raggio interno solenoide [m]
D_cm = 2*((r_c_ext - r_c_int)/2)+r_c_int); %diametro medio solenoide [m]
l_c = 27.9e-3; %altezza solenoide [m]
A_c = (r_c_ext-r_c_int)*l_c;%Area trasversale metà solenoide [m^2]

%Ampere-Spire
AS=644; %[A]

%Filo
D_w = [.56e-3 .8e-3 1.3e-3]; %Diameter nude wire[m]
D_ws = [.225e-3 .425e-3 .585e-3 .825e-3 1.325e-3]; %Diameter smalleted wire[m]
S_w = (pi*D_w.^2)/4; %sezione filo [m^2]
N = 280; %numero avvolgimenti
l_w = pi*N*(r_c_int+(12*D_w)); %lunghezza filo utilizzato nella bobina[m]
l_wextra = l_w + 0.2; %lunghezza totale filo
W_w = Cu_dens*l_wextra.*S_w; %Totale weight of the Copper wire

%% Spazio occupato dal filo
N_ffs = l_c./D_ws; %massimo numero di fili per strato
A_occ_id = N.*S_w; %area trasv. ideale occupata dal filo
A_occ = A_occ_id.*((4/pi)); %area trasv. occ. con fattore d'impacchettamento
SF = A_occ./A_c; %space factor, indica la percentuale di area disponibile utilizzata

```

```

%% Ohm's Laws
R = (rho*l_wextra)./S_w; %Coil Resistance [Ohm]
i0 = AS/N; %corrente a regime [A]
V = R.*i0; %voltage [V]
P = R.*i0.^2; %potenza [W]
j = i0./(S_w*10^6); %DensitÀ di corrente [A/mm^2] j limite 6A x mmq

%% Temperature filo, caso adiabatico (pochi secondi)
T_fus = 900; %T accettabile rame (T fusione 1086)
DT = T_fus - T; %Delta T accettabile
rho2 = 0.0156*(1 + 0.00428*T_fus)*1e-6; %Cu resistivity[Ohm*(m)]
R2 = (rho2*l_wextra)./S_w; %Coil Resistance [Ohm]
CS = 385; %Calore specifico Rame [J/(kg*Â°C)]
t_fus = (CS*W_w*DT)./(R2*(i0.^2));

%% Induttanza & Tempo risposta
mu_v = 15000; %vacoflux relative permeability[H/m]
mu_0 = pi*4e-7; %vacuum permeability[H/m]
mu_rel = 500; %circuit relative permeability[]
D_core = 4.05e-3; %diametro nucleo in vacoflux [m]
S_core = (pi*D_core.^2)/4; %sezione nucleo vacoflux [m^2]
L = (mu_v*mu_0*S_core*(N).^2)/l_c; %inductance [H]
tau=(L./R)*1000; %circuit time constant [ms]
tau_r= 5*tau; %circuit time response [ms]

%% Magnetic Circuit's Geometry%%
l_0max = 0.625e-3; %max air gap
l_0min = 0.4e-3; %min air gap
A_0 = (((pi*(.0155^2 - .001^2))/4) + ((pi*(.004^2 - .001^2))/4))/2; %Air gap Sect
l_1 = .0285; %lenght of FerroCore [m]

```

```

A_1 = (pi*(.004^2 - .001^2))/4; %Section Ferrocore [m^2]
l_2 = .0042; %length of PusheMag1 [m]
A_2 = (pi*(.0155^2 - .001^2))/4; %Section PusheMag1 [m^2]
l_3 = .005; %length of PushrMag2 [m]
A_3 = (pi*(.0025^2 - .0006^2))/4;%Section PushrMag2 [m^2]
l_4 = .05; %length of External Circuit [m]
A_4 = (pi* .01^2); %Section External Circuit [m^2]

%% Reluctances%%
Rel_0 = l_0max/(mu_0*A_0); %Max Air gap reluctance [1/H]
Rel_1 = l_1/(mu_0*mu_v*A_1); %Part 1 reluctance [1/H]
Rel_2 = l_2/(mu_0*mu_v*A_2); %Part 2 reluctance [1/H]
Rel_3 = l_3/(mu_0*mu_v*A_3); %Part 3 reluctance [1/H]
Rel_4 = l_4/(mu_0*mu_rel*A_4); %Part 4 reluctance [1/H]
Rel_tot = Rel_0 + Rel_1 + Rel_2 + Rel_3 + Rel_4; %Total Reluctance [1/H]

%% Empirical coefficent
phiE = 0.97/8.59;

%% Magnetic flux,field and induction%%
phi = phiE*N.*i0/Rel_tot; %Magnetic flux [Wb]
B_0 = phi/A_0; %Flux density through Air gap [T]
B_1 = phi/A_1; %Flux density through part 1 [T]
B_2 = phi/A_2; %Flux density through part 2 [T]
B_3 = phi/A_3; %Flux density through part 3 [T]
H_0 = B_0/mu_0; %Magnetic Field through Air gap [A/m]
H_1 = B_1/(mu_0*mu_v); %Magnetic Field through part 1 [A/m]
H_2 = B_2/(mu_0*mu_v); %Magnetic Field through part 2 [A/m]
H_3 = B_3/(mu_0*mu_v); %Magnetic Field through part 3 [A/m]

%% Magnetic Force%%

```

```

F_minairgap = ((phiE*(N.*i0).^2)*mu_0*S_core)/(2*(l_0min)^2); %Max Magnetic Force
F_maxairgap = ((phiE*(N.*i0).^2)*mu_0*S_core)/(2*(l_0max)^2); %Min Magnetic Force

%% Display Results
disp(' ')
disp('Ampere-Spire [A]:' ,num2str(AS), ''))
disp(' ')
disp(['Number of turns:' ,num2str(N), ''])
disp(' ')
disp(['Diametro filo [mm]' ,num2str(1000*D_w), ''])
disp(' ')
disp(['Lenght of the wire [m]' ,num2str(l_w), ''])
disp(' ')
disp(['Weight of the wire [g]' ,num2str(W_w*10^3), ''])
disp(' ')
disp(['Space Factor [%]' ,num2str(SF), ''])
disp(' ')
disp(['Power [W]' ,num2str(P), ''])
disp(' ')
disp(['Voltage [V]' ,num2str(V), ''])
disp(' ')
disp(['Resistance [Ohm]' ,num2str(R), ''])
disp(' ')
disp(['Current [A]' ,num2str(i0), ''])
disp(' ')
disp(['Current Density [A/mm^2]' ,num2str(j), ''])
disp(' ')
disp(['Time to fusion [s]' ,num2str(t_fus), ''])
disp(' ')

```

```

disp(['Inductance [H]: ',num2str(L), ''])
disp(' ')
disp(['Time constant [ms]: ',num2str(tau), ''])
disp(' ')
disp(['Time for 99% saturation [ms]: ',num2str(tau_r), ''])
disp(''')
disp(''')
disp(''')
disp(''')
disp(['Total Reluctance [1/H]: ',num2str(Rel_tot), ''])
disp(' ')
disp(['Traferrro Reluctance [1/H]: ',num2str(Rel_0), ''])
disp(' ')
disp(['Flux density through Air gap [T]: ',num2str(B_0), ''])
disp(' ')
disp(['Flux density through part 1 [T]: ',num2str(B_1), ''])
disp(' ')
disp(['Flux density through part 2 [T]: ',num2str(B_2), ''])
disp(' ')
disp(['Flux density through part 3 [T]: ',num2str(B_3), ''])
disp(' ')
disp(['Magnetic Field through 0 [A/m]: ',num2str(H_0), ''])
disp(' ')
disp(['Magnetic Field through 1 [A/m]: ',num2str(H_1), ''])
disp(' ')
disp(['Magnetic Field through 2 [A/m]: ',num2str(H_2), ''])
disp(' ')
disp(['Magnetic Field through 3 [A/m]: ',num2str(H_3), ''])
disp(' ')
disp(['Max Magnetic Force [N]: ',num2str(F_minairgap), ''])
disp(' ')

```

```
disp(['Min Magnetic Force [N]: ',num2str(F_maxairgap), '])  
disp('
```

Bibliography

- [1] A. N. Mansfield, "*Electromagnets: their design and construction*", Nosstrand Company, 1901.
- [2] Serway, Jewett "*Physics for Scientists and Engineers*", Brooks/Cole, 2014.
- [3] Jack Tanabe , "*Iron Dominated Electromagnets Design, Fabrication, Assembly and Measurements*", Stanford, 2005.
- [4] Sergio Barsali, G. Carlo Barsotti, Umberto Rosa, "*Lezioni di Disegno di Macchine*", San Marco Litotipo, 1993.
- [5] Jaecheol Koh, "*CATIA V5 Design Fundamentals: A Step by Step Guide*", Onsia, 2012.
- [6] John F. O'Hanlon, "*A User's Guide to Vacuum Technology*", Whley, 2003.
- [7] Robert C. Juvinall, Kurt M. Marshek, "*Machine Component Design*", Wiley Indian Edition, 2012.
- [8] Shigley, "*Progetto e Costruzione di Macchine*", McGraw-Hill, 1963.
- [9] Walter Umbrath, "*Fundamentals of Vacuum Technology*", Leybold, Cologne, June 2007.
- [10] M. F. Samadi, M. Saif, "*Approach control of an Electromechanical Valve Actuator Using Closed-loop Iterative Learning Control*", Paper presented

at 50th IEEE Conference on Decision and Control and European Control Conference (CDC-ECC) Orlando, FL, USA, December 12-15, 2011.

- [11] A. E. Hajjaji, M Ouladsine, "*Modeling and Nonlinear Control of Magnetic Levitation Systems*", Paper presented at IEEE TRANSACTIONS ON INDUSTRIAL ELECTRONICS, VOL. 48, NO. 4, AUGUST 2001.
- [12] C. Tai, A. Stubbs, T. Tsao, "*Modeling and Controller Design of an Electromagnetic Engine Valve*", Paper presented at the American Control Conference Arlington, VA June 25-27, 2001.
- [13] C. Koch, A. Lynch, R. Chladny, "*Modeling and control of solenoid valves for internal combustion engines*", Paper presented at the 2nd International Federation of Automatic Control (IFAC) Conference on Mechatronic Systems, 2002.
- [14] E. D. Bushway, R. Perini, "*Proportional Flow Control Valve (PFCV) for Electric Propulsion System*", Papers presented for the 3rd International Conference on Spacecraft Propulsion, Cannes, 10-13 October, 2000.
- [15] P. T. King, E. D. Bushway, "*A Xenon Flowrate Controller for Hall Current Thruster Applications*", Moog Inc., 2001.
- [16] D. M. Pehrson, "*Continuing Development of the Proportional Flow Control Valve (PFCV) for Electric Propulsion System*", Paper presented at the 30th International Electric Propulsion Conference, Florence, Italy, September 17-20, 2007.
- [17] C. Weddle and D. Leo, "*Embedded actuation systems for camless engines*", Paper presented at the Int. Conf. on Adaptive Structures and Technologies, Boston, MA, Oct. 14-16, 1998.
- [18] Ray Thompson, Howard Gray , "*The Xenon Regulator and Feed System For Electric Propulsion Systems*", Paper presented at the 29th International Electric Propulsion Conference, Princeton University, October 31 - November 4, 2005.

- [19] Y. Kim, S. Kang, Y. Jeong, J. Seon, J. Wee, H. Yoon, J. Lee, M. Seo, W. Choi, "*Development of Xenon feed system for a 300-W Hall-Thruster*", Paper presented at the 31st International Electric Propulsion Conference, University of Michigan, Ann Arbor, Michigan, USA, September 20 - 24, 2009.
- [20] J. R. Beattie, R. R. Robson, J. D. Williams, "*18-mN Xenon Ion Propulsion Subsystem*", Hughes Research Laboratories, Malibu, California 90265, USA, 1991.
- [21] R. Shotwell, B. Butler, D. Bushway, D. Perini, S. Gross, R. Kelly, "*Evaluation of Proportional Flow Control Valve for Potential Use in Electric Propulsion System*", American Institute of Aeronautics and Astronautics, 1999.
- [22] S. Sastry, "*Nonlinear Systems: Analysis, Stability, and Control*", New York: Springer-Verlag, 1999.
- [23] T. Parlikar, W. Chang, Y. Qiu, M. Seeman, D. Perreault, J. Kassakian, T. Keim, "*Design and experimental implementation of an electromagnetic engine valve drive*", IEEE/ASME Transactions on Mechatronics, 2005.

